



저작자표시-비영리-변경금지 2.0 대한민국

이용자는 아래의 조건을 따르는 경우에 한하여 자유롭게

- 이 저작물을 복제, 배포, 전송, 전시, 공연 및 방송할 수 있습니다.

다음과 같은 조건을 따라야 합니다:



저작자표시. 귀하는 원저작자를 표시하여야 합니다.



비영리. 귀하는 이 저작물을 영리 목적으로 이용할 수 없습니다.



변경금지. 귀하는 이 저작물을 개작, 변형 또는 가공할 수 없습니다.

- 귀하는, 이 저작물의 재이용이나 배포의 경우, 이 저작물에 적용된 이용허락조건을 명확하게 나타내어야 합니다.
- 저작권자로부터 별도의 허가를 받으면 이러한 조건들은 적용되지 않습니다.

저작권법에 따른 이용자의 권리는 위의 내용에 의하여 영향을 받지 않습니다.

이것은 [이용허락규약\(Legal Code\)](#)을 이해하기 쉽게 요약한 것입니다.

[Disclaimer](#)

Thesis for the Degree of Master of Science

Development of an Electrochemical
Sensor for Quantitative Detection of
Chemically Converted Biliverdin: Toward
Point-of-Care Diagnosis of
Hyperbilirubinemia

by

Khan Md Mahbubur Rahman

Industry 4.0 Convergence Bionics Engineering

The Graduate School

Pukyong National University

August, 2025

Development of an Electrochemical
Sensor for Quantitative Detection of
Chemically Converted Biliverdin: Toward
Point-of-Care Diagnosis of
Hyperbilirubinemia

(현장 진단용 고빌리루빈혈증 검출을 위한
화학적 전환 빌리베르딘의 정량 분석 전기
화학 센서 개발)

Advisor: Prof. Joong Ho Shin

by

Khan Md Mahbubur Rahman

A thesis submitted in partial fulfillment of the requirements for the degree of
Master of Science
in Industry 4.0 Convergence Bionics Engineering, The Graduate School,
Pukyong National University

August, 2025

Development of an Electrochemical Sensor for Quantitative
Detection of Chemically Converted Biliverdin: Toward Point-of-
Care Diagnosis of Hyperbilirubinemia

A dissertation

by

Khan Md Mahbubur Rahman

Approved by:



Prof. Yong Wook Lee, PhD.
(Chairman)

Prof. Songyi Lee, PhD.
(Member)

Prof. Joong Ho Shin, PhD.
(Member)

August. 22. 2025

Table of Contents

Table of Contents.....	i
List of Tables.....	iv
List of Figures.....	v
List of Abbreviations.....	viii
Abstract.....	xi
1. Introduction.....	1
1.1. Research Background.....	1
1.2. Related Research Trend.....	4
1.3. Research Purpose.....	6
2. Conceptual Overview.....	7
2.1. Bilirubin Chemical Oxidation Reaction.....	7
2.2. Fabrication of PABA-Modified SPE.....	9
2.3. Electrochemical Analysis of Biliverdin using SPE/PABA.....	10
3. Materials and Experimental.....	11
3.1. Chemicals and Reagents.....	11
3.2. Instrumentation.....	11
3.3. Au³⁺-Assisted Bilirubin Oxidation.....	12
3.3.1. UV-Vis Spectroscopy Analysis.....	12
3.3.2. LC-MS/MS Analysis.....	13
3.4. Electrochemical Polymerization of 4-ABA into PABA.....	14
3.5. Electrochemical Investigation of SPE/PABA.....	15
3.5.1. Cyclic Voltammetry (CV).....	15
3.5.2. Electrochemical Impedance Spectroscopy (EIS).....	15

3.6. Physicochemical Characterization of SPE/PABA	16
3.6.1. Field Emission Scanning Electron Microscopy (FE-SEM) ..	16
3.6.2. Raman Spectroscopy	17
3.6.3. X-ray Photoelectron Spectroscopy (XPS)	17
3.7. Electrochemical Oxidation of Biliverdin using SPE/PABA	18
3.7.1. pH Effect on Electrochemical Oxidation of Biliverdin	18
3.7.2. Cyclic Voltammetry	18
3.7.3. Amperometry	19
3.8. Specificity Study	20
3.9. Stability and Reproducibility	21
3.10. Recovery Study	22
3.11. Real Sample Analysis	22
3.12. Comparison of Electrochemical Method and Standard Method	23
4. Results and Discussion	24
4.1. Analysis of Bilirubin Oxidation Reaction	24
4.1.1. UV-Vis Spectroscopy Analysis	24
4.1.2. LC-MS/MS Analysis	26
4.2. Electrochemical Investigation of SPE/PABA	27
4.2.1. Cyclic Voltammetry (CV)	27
4.2.2. Electrochemical Impedance Spectroscopy (EIS)	31
4.3. Physicochemical Characterization of SPE/PABA	32
4.3.1. Field Emission Scanning Electron Microscopy (FE-SEM) ..	32
4.3.2. Raman Spectroscopy	33
4.3.3. X-ray Photoelectron Spectroscopy (XPS)	34
4.4. Electrochemical Oxidation of Biliverdin at SPE/PABA Electrode	37

4.4.1. pH Effect on Electrochemical Oxidation of Biliverdin	37
4.4.2. Cyclic Voltammetry	39
4.5. Amperometry	40
4.6. Specificity Study	42
4.7. Stability and Reproducibility	44
4.8. Recovery Study	45
4.9. Real Sample Analysis	47
4.10. Comparison of Electrochemical Method and Standard Method	48
5. Conclusions	50
6. Reference	52



List of Tables

Table 1. Performance comparison with other nonenzymatic electrochemical bilirubin sensors.	42
Table 2. Recovery performance measurement for the added BV using SPE/PABA.	46
Table 3. Comparison of BV sensing performance in spiked human serum samples using SPE/PABA and UV-vis. method.	50



List of Figures

Fig. 1. Operating principle of an electrochemical sensor	2
Fig. 2. Schematic illustrations of (A) Cyclic voltammetry showing redox behavior during potential scanning, and (B) Amperometry depicting current response after sample addition.....	4
Fig. 3. Schematic representation of bilirubin oxidation and the fabrication of PABA modified SPE for electrochemical biliverdin sensing.....	7
Fig. 4. Bilirubin oxidation reaction mechanism.	8
Fig. 5. Electropolymerization mechanism of 4-aminobenzoic acid (4-ABA)...	9
Fig. 6. Photograph of (A) BR oxidation reaction mixture and (B) Reaction mixtures with variable BR concentrations.....	13
Fig. 7. UV-visible spectrum of (A) Ethanolic solution of gold chloride, (B) Ethanolic solution of BR, and (C) After completion of the reaction mixture of Au ³⁺ and BR.....	24
Fig. 8. UV-visible spectrum (A) Absorbance spectra with variable BR concentrations (10 to 70 μ M) and (B) Time-dependent absorbance curve at 700 nm. The reactions were performed in the presence of gold (III) chloride (100 μ M) in an ethanolic solution.	25
Fig. 9. LC-MS/MS chromatograms of standard biliverdin (blue chromatogram) and the reaction product (red chromatogram). Both compounds eluted at a retention time of 4.35 min, confirming that the product formed in the reaction matches the standard biliverdin.....	27
Fig. 10. CV curves were recorded using SPE/PABA modified electrodes in 0.1 M HCl at 25 mV s ⁻¹ . The Inset label indicates the various cycling scans (5, 10, 15 and 20 scans) during the polymerization of PABA on SPE.....	28
Fig. 11. Electrochemical polymerization on SPE in 0.05 M HCl with 3 mM 4-	

ABA at 0.025 V/s over ten cycling scans.....	29
Fig. 12. CV response obtained using SPE/PABA in variable pH buffered solution containing 5 mM of K ₄ [FeCN ₆]/ K ₃ [FeCN ₆].	30
Fig. 13. EIS curves obtained using SPE/PABA in variable pH buffered solution containing 5 mM of K ₄ [FeCN ₆]/ K ₃ [FeCN ₆], Inset of (A) is the equivalent circuit obtained from fitting, and (B) shows the Effect of pH on Rct.....	31
Fig. 14. Physicochemical characterization of the modified electrode. (A) FESEM images of SPE and (B) SPE/PABA electrode; Inset of the fig. (A and B): Elemental analysis. (C) Elemental mapping of the SPE/PABA electrode.	32
Fig. 15. Raman shift of SPE (red curve) and SPE/PABA (blue curve) surfaces.	34
Fig. 16. XPS spectra of SPE electrode (working electrode surface). (A) Survey scan, (B) and (C) High-resolution deconvoluted spectra of C1s and O1s.	35
Fig. 17. (A) XPS Survey Scan of SPE/PABA and deconvoluted XPS spectrum of (B) C1s (C) O1s, and (D) N1s.	36
Fig. 18. Electrochemical oxidation of BV at the SPE/PABA electrode. (A) CV responses of SPE/PABA electrode in buffer with variable pH containing 150 μM of BV. (B) Effect of pH on peak potential and peak current.....	37
Fig. 19. Electrochemical oxidation of BV at the SPE/PABA electrode. (A) CV responses for a & c in the presence of BR (100 μM), b & d in the presence of BV (100 μM) using SPE and SPE/PABA electrode, and the dotted line correspondence to control CV curve, and (B) CV responses of SPE/PABA modified electrode in Tris-HCL (pH = 8.5) with variable concentrations of BV (0, 10, 20, 50, 200, 300, and 400 μM) at 25 mV s ⁻¹ (Inset shows enlarged view of CV curves).....	39
Fig. 20. Electrochemical sensing performance. (A) I–t response recorded using SPE/PABA electrode in the presence of BV concentrations (5 to 440 μM) at 0.32	

V and (B) Linearity plot obtained from I-t curves.	40
Fig. 21. Electrochemical sensing performance. (A) Selectivity study from I-t response recorded using SPE/PABA electrode with possible electroactive biomolecules, and (B) Histogram representing the relative percentage of current.	43
Fig. 22. I-t response curve recorded for (A) Stability (repeatability) and (B) Reproducibility of SPE/PABA modified electrode in Tris-HCl (pH – 8.5) containing BV at 0.32 V.	44
Fig. 23. I-t response curve recorded for variable BV concentration in Tris-HCl (pH 8.5) at 0.32 V.	46
Fig. 24. Electrochemical sensing performance of SPE/PABA in BV-spiked human serum.	47
Fig. 25. UV-visible absorbance spectra for (A) Different concentrations (1 to 180 μ M) of standard biliverdin, (B) Linearity plot obtained from UV-spectrum, and (C) UV-vis spectral curve recorded for human serum spiked with BV (reaction mixture).	49

List of Abbreviations

BR	Bilirubin
BV	Biliverdin
PABA	Poly-aminobenzoic acid
4-ABA	4-aminobenzoic acid
Au ³⁺	Gold (III) ion
SPE	Screen-printed electrode
SPE/PABA	Poly(aminobenzoic acid) modified screen-printed electrode
MIP	Molecularly imprinted polymer
COOH-	Carboxylated multi-walled carbon nanotubes
MWCNT	
LOD	Limit of detection
FET	Field-effect transistor
GNH	Graphene nanohybrid
MnO ₂	Manganese dioxide
BOx	<i>Bilirubin oxidase</i>
AuNPs	Gold nanoparticles
KCl	Potassium chloride

CV	Cyclic voltammetry
HCl	Hydrochloric acid
N ₂	Nitrogen gas
EIS	Electrochemical impedance spectroscopy
OCP	Open circuit potential
λ _{max}	Wavelength of Maximum Absorbance
m/z	Mass-to-Charge Ratio
RT	Retention time
R _{ct}	Charge transfer resistance
I _D /I _G	Intensity ratio of D-band to G-band
PP	Purpurin
Ch	Choletelin
PCET	Proton-coupled electron transfer
I _p _a	Anodic peak current
I-t	Current versus time (Amperometric response curve)

Development of an Electrochemical Sensor for Quantitative Detection of Chemically
Converted Biliverdin: Toward Point-of-Care Diagnosis of Hyperbilirubinemia

Khan Md Mahbubur Rahman

Industry 4.0 Convergence Bionics Engineering, Pukyong National University

Abstract

Bilirubin (BR)은 간 기능 및 관련 질환 진단에 있어 중요한 바이오마커로 알려져 있음. 그러나 BR은 낮은 수용성과 전극 오염 특성으로 인해 기존의 전기화학적 검출 방식에 한계가 있음. 본 연구에서는 삼가 금이온을(Au^{3+})을 이용한 BR의 산화 반응을 통해 생성된 Biliverdin (BV)을 기반으로 하는 새로운 전기화학 분석 전략을 제안함. BR 산화 반응은 자외선-가시광선(UV-Vis) 분광법을 통해 분석되었으며, Au^{3+} 는 BR 대비 1.67의 몰비에서 3분 이내에 완전 산화를 유도하는 효과적인 산화제로 확인됨. 생성된 BV는 폴리(아미노벤조산)(PABA)로 기능화된 스크린 프린팅 탄소 전극(SPE)을 이용하여 순환 전압전류법(CV)과 암페로메트리 분석으로 전기화학적으로 조사됨. SPE/PABA 전극은 전위-동적 기법으로 제작되었으며, 물리화학적 및 전기화학적 특성 분석을 통해 평가됨. BV는 pH 8.5 완충 용액에서 0.32 V에서 산화되었으며, 해당 센서는 선택적인 BV 산화, 낮은 전극 오염, 그리고 넓은 농도 검출 범위를 나타냄. 감도는 $0.115 \mu A \mu M^{-1} cm^{-2}$, 선형 검출 범위는 5–440 μM , 검출 한계(LOD)는 0.9 μM 으로 측정되었음. 또한, 본 연구에서 개발한 센서는 전기활성 가능성이 있는 생체분자가

존재하는 조건에서도 우수한 재현성과 높은 선택성을 입증함. 인체 혈청 첨가 샘플 분석에서도 유의미한 결과를 도출하였으며, 빌리루빈 관련 질환의 진단에 활용될 수 있는 가능성을 제시함.



1. Introduction

1.1. Research Background

Bilirubin (BR) ($C_{33}H_{36}N_4O_6$) is a tetrapyrrolic bile pigment produced from the breakdown of heme. In human serum, it exists in two forms: unconjugated bilirubin and conjugated bilirubin. Unconjugated bilirubin (UBR) is a nonpolar, water-insoluble molecule that circulates in the bloodstream bound to serum albumin, and this binding can be readily cleaved by anionic detergents or organic solvents [1,2]. Usually, BR is metabolized in the liver, where it couples with glucuronic acid to generate water-soluble bilirubin glucuronides. These substances are excreted in bile and subsequently removed from the intestines. Bilirubin converts into urobilinogen by gut bacteria in the intestines, where it can be converted into stercobilin afterwards and excreted with feces [3]. A portion of urobilinogen is eliminated in urine after being reabsorbed into the circulation. Low bilirubin levels have been linked to iron deficiency anemia and an increased risk of coronary artery disease, whereas elevated levels can contribute to metabolic disorders and conditions such as hepatitis and kernicterus [4]. Normally, total serum bilirubin ranges from 0.3 to 1.9 mg/dL [5]. Abnormal bilirubin metabolism might potentially impact infants and have serious health consequences on adults, which might lead to death, brain damage, and liver illness [6].

Since BR was first detected in blood in 1847, several methods have been developed for its measurement. Among them, the spectrophotometric method introduced by Jendrassik and Grof remains widely used for determining BR levels in blood and plasma. Spectrophotometric analysis of newborn serum offers a simple and rapid procedure requiring minimal sample volumes; however, the diazo-reaction technique suffers from pH dependence and susceptibility to interference by other biomolecules, reducing its precision in real sample analysis [7]. In recent decades, advanced techniques such as chemiluminescence, polarography, and fluorometry have been introduced, utilizing detection principles based on light emission, electrochemical

properties, and fluorescence, respectively. While these methods offer distinct advantages, they also face notable limitations, including inconsistency in quantitative analysis, interference from biological components, and relatively low sensitivity [2]. Consequently, there is a significant clinical demand for BR testing methods that are faster, more sensitive, and more specific than earlier approaches. Real-time monitoring of BR levels is crucial for assessing liver function, and rapid, user-friendly point-of-care devices can minimize unnecessary clinical visits, empower patients, and enable timely clinical decision-making [8,9].

Electrochemical biosensors, in particular, offer the potential advantages of providing affordable, portable devices suitable for emergency applications in remote or resource-limited settings. These sensors integrate biological or biologically derived components with a transducing microsystem to generate an electrochemical signal upon interaction with the target analyte. Electrochemical biosensors can be broadly categorized into amperometric, potentiometric, and impedimetric types, depending on the measured electrochemical parameter, such as current, potential, or impedance, respectively [10].

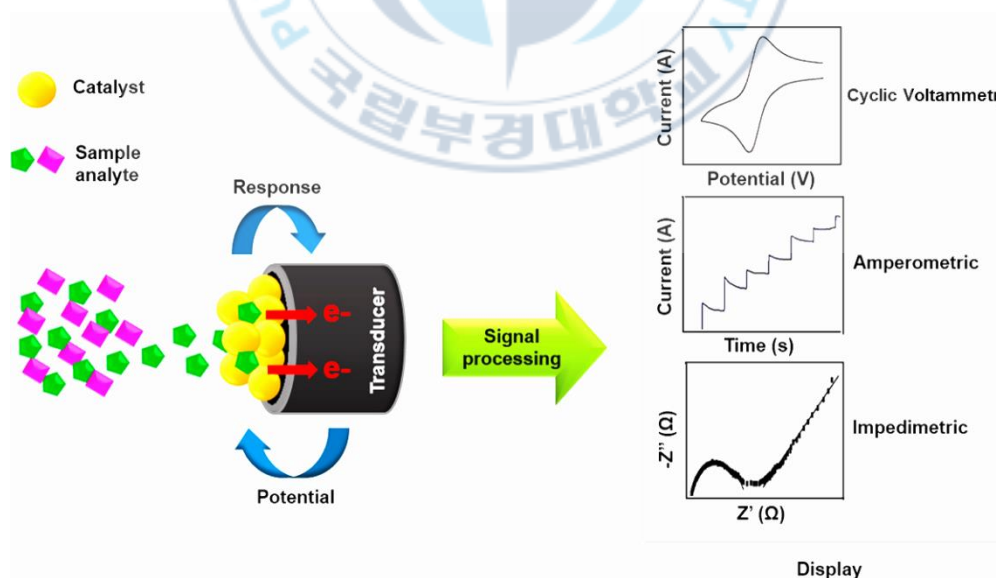


Fig. 1. Operating principle of an electrochemical sensor

Fig. 1 illustrates the fundamental operating principle of an electrochemical sensor, where sample analytes interact with a catalyst-modified electrode, inducing redox reactions that generate measurable signals. When an external potential is applied, electrons are transferred between the working electrode and the analyte. A positive potential drives oxidation (electron flow from analyte to electrode), while a negative potential induces reduction (electron flow from electrode to analyte); by convention, oxidation occurs at the anode and reduction at the cathode. These electron transfer processes are detected and processed by the transducer, with outputs visualized through various electrochemical techniques [11,12]. For example, cyclic voltammetry (CV) provides redox profiles by sweeping the potential range, amperometry measures real-time current at a fixed potential, and electrochemical impedance spectroscopy (EIS) evaluates interfacial properties via frequency-based impedance measurements. Together, these methods enable sensitive, selective, and rapid analysis of electroactive species in diverse biosensing applications [13].

Cyclic voltammetry (CV) is one of the most fundamental and versatile techniques used to evaluate the electrochemical properties of a molecule. It allows researchers to scan the potential across a defined range while measuring the resulting current, providing valuable information on oxidation and reduction potentials, reaction reversibility, and electron transfer kinetics [14]. CV is especially useful in determining the redox behavior of electroactive species and identifying an appropriate working potential for further quantitative analysis. Fig. 2(A) illustrates the basic principle of cyclic voltammetry, where the current is measured during a forward and reverse potential scan, revealing distinct oxidation and reduction peaks corresponding to redox processes. Whereas amperometry involves applying a fixed potential to the working electrode and recording the resulting faradaic current over time. Because the non-faradaic (capacitive) current decays rapidly, amperometry enables selective measurement of the steady-state faradaic current, making it ideal for quantitative sensing applications such as calibration curve generation and detection limit analysis [15]. Fig. 2(B) shows the amperometric response, where the current increases after

sample addition at a fixed potential and reaches a steady-state plateau, indicating the oxidation of the analyte.

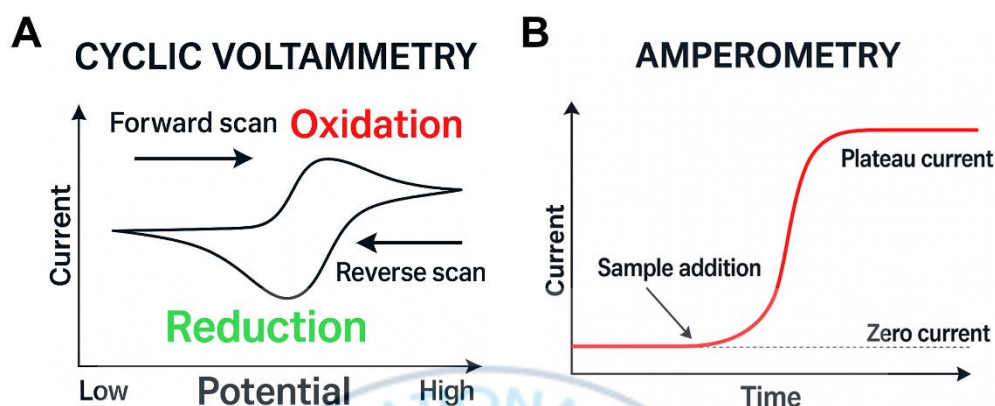


Fig. 2. Schematic illustrations of (A) Cyclic voltammetry showing redox behavior during potential scanning, and (B) Amperometry depicting current response after sample addition.

In this study, CV was employed to explore the redox characteristics of biliverdin and determine its oxidation potential, which informed the selection of the fixed potential used in amperometric measurements. Amperometry was subsequently used to construct the calibration curve, as it allows for sensitive and reproducible quantification of BV concentrations by measuring current responses under controlled potential conditions. The accurate detection and quantification of BR are critical for clinical diagnostics, necessitating the development of reliable analytical devices.

1.2. Related Research Trend

Recently, electrochemical sensors have emerged as promising alternatives for BR detection due to their simplicity, selectivity, and compatibility with miniaturized and point-of-care platforms. Unlike conventional spectrophotometric and enzyme-

based assays-which are limited by pH sensitivity, high operational cost, and poor stability-electrochemical approaches offer rapid, cost-effective, and portable detection systems. Among recent innovations, nanomaterial-assisted molecularly imprinted polymer (MIP) sensors have demonstrated significant improvements in sensitivity and stability. For example, Manoj et al. developed a $\text{Ti}_3\text{C}_2\text{T}_x$ MXene-modified ITO electrode using a polypyrrole-based MIP layer, achieving improved BR detection via enhanced film integrity and electrocatalytic response [16]. In a subsequent study, the same group integrated MXene with carboxylated multi-walled carbon nanotubes (COOH-MWCNT) and MIP-electropolymerized o-phenylenediamine, reaching an ultra-low detection limit (LOD) of 0.002 mg/dL while maintaining high selectivity and reusability in serum samples [17]. Similarly, Bui et al. introduced a printable field-effect transistor (FET) sensor using GNH/MnO₂ composites, combining MnO₂'s catalytic activity and graphene oxide's conductivity to achieve femtomolar sensitivity [18]. Kumar et al. reported a graphene oxide/polypyrrole/polyaniline/zinc oxide nanocomposite sensor with high conductivity and structural stability [19]. Despite these promising advancements, MIP-based electrochemical sensors still face challenges such as narrow linear ranges, high detection limits, non-uniform imprinting, and complex fabrication procedures, which hinder their clinical applicability. This reinforces the need for BR detection methods that are not only sensitive and selective but also scalable, cost-effective, and robust. In this context, electrochemical sensors-particularly those based on screen-printed electrodes (SPEs)-have shown great potential. SPEs offer low cost, flexibility in design, integrated three-electrode configurations, and excellent reproducibility, making them highly suitable for portable BR sensing in decentralized and resource-limited environments [8,9].

The first mechanism for the electrochemical oxidation of BR to biliverdin was proposed by Slifstein and Ariel in 1973, marking the earliest attempt to characterize this redox transformation [20]. Following this, enzyme-based electrochemical sensing, particularly using bilirubin oxidase (BOx), gained widespread attention due to the enzyme's specificity for BR under physiological conditions [21]. However, these

sensors are limited by high cost, instability, and challenges associated with enzyme immobilization. As a result, nonenzymatic sensors based on nanomaterials have gained attention for their chemical stability, electrocatalytic activity, and affordability. Materials such as gold nanostructures, conducting polymers, graphene, carbon nanotubes, and metal oxides-and their composites with noble metals-have been explored as enzyme-free alternatives [22,23]. Nevertheless, direct electrochemical detection of BR remains challenging due to surface fouling, primarily caused by BR passivation or polymerization on the electrode surface [24]. To address this issue, Thangavel et al. proposed surface modification with poly(aminobenzoic acid) (PABA), an anionic polymer that prevents BR adsorption and improves signal stability. PABA-functionalized electrodes create a negatively charged surface that minimizes fouling and enables more reliable electrochemical sensing [25]. Moreover, Edachana et al. reported a colorimetric assay in which BR reduces Au^{3+} to form gold nanoparticles (AuNPs), resulting in a visible color change [26]. However, this method lacks quantitative precision, and the role of BV formation remains underexplored. Given that BV is electrochemically active and forms stoichiometrically from BR during redox reactions, this study focuses on chemically oxidizing BR to BV using Au^{3+} and quantifying BV electrochemically. This indirect approach allows for a more reliable, specific, and sensitive method for BR analysis using PABA-modified SPEs.

1.3. Research Purpose

In response, this study proposes an indirect electrochemical detection strategy by investigating the electrochemical oxidation of biliverdin, which was obtained from the Au^{3+} -assisted BR chemical oxidation. BR was chemically oxidized using Au^{3+} in an ethanolic medium, and the generation of BV was confirmed by UV–Vis spectroscopy and cyclic voltammetry. The resulting BV was quantitatively analyzed using a screen-printed carbon electrode functionalized with poly(aminobenzoic acid), which provides

antifouling properties and enhances electrocatalytic activity. CV was used to identify the oxidation potential of BV, followed by amperometric measurements to construct the calibration curve. This indirect sensing approach overcomes key limitations of direct BR detection by reducing electrode fouling and enhancing signal stability, while maintaining a reliable stoichiometric link to BR levels. The sensor was systematically evaluated for sensitivity, linearity, reproducibility, and performance in human serum samples. Overall, the proposed platform demonstrates significant selectivity, high sensitivity with a wide linear range, and human serum analysis, which indicates its potential application method for point-of-care bilirubin diagnostics.

2. Conceptual Overview

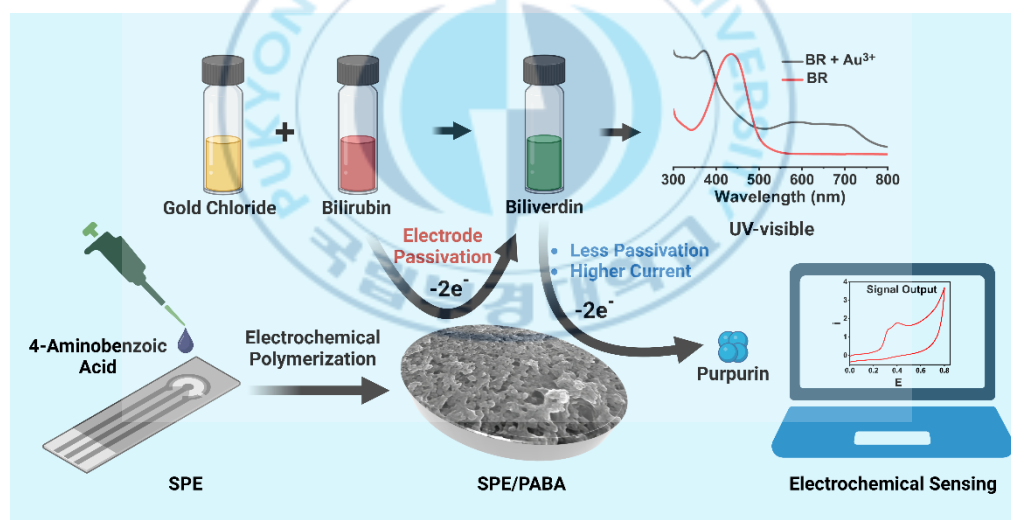


Fig. 3. Schematic representation of bilirubin oxidation and the fabrication of PABA modified SPE for electrochemical biliverdin sensing.

2.1. Bilirubin Chemical Oxidation Reaction

This study introduces an indirect sensing strategy in which BR is first

chemically oxidized to biliverdin, which is then detected electrochemically. The oxidation of BR was carried out using gold(III) chloride (AuCl_3) in an ethanolic medium, and the formation of BV was confirmed using UV–Visible spectroscopy and cyclic voltammetry (CV). During this redox reaction, BR donates electrons to Au^{3+} , which reduces Au^{3+} to gold nanoparticles (AuNPs), and BR is converted into its oxidized form, BV. Direct detection of BR using bare carbon electrodes is often hindered by strong adsorption of BR onto the electrode surface, leading to fouling and a decline in sensitivity, particularly at higher BR concentrations.

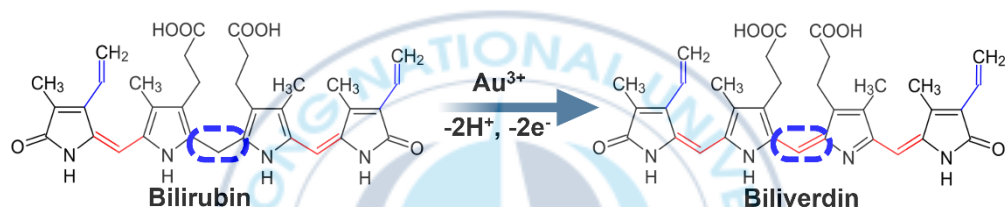


Fig. 4. Bilirubin oxidation reaction mechanism.

Although BR oxidizes at a lower potential (~ 0.2 V), it causes significant signal instability. In contrast, BV oxidizes at a slightly higher potential (~ 0.32 V) but produces a stronger and more stable oxidation signal with reduced fouling, making it a more suitable analyte for electrochemical analysis. As BV is stoichiometrically related to BR in this controlled oxidation reaction, its concentration can be directly correlated to BR levels. This allows BV to act as a proxy for BR quantification, thus improving the selectivity and reproducibility of the sensor system for potential clinical diagnostic applications.

2.2. Fabrication of PABA-Modified SPE

To enhance the performance of BV detection, the surface of the screen-printed carbon electrode (SPE) was modified with poly(aminobenzoic acid) (PABA) via electropolymerization of 4-aminobenzoic acid (4-ABA) (Fig. 5). The use of SPEs offers advantages such as low cost, ease of modification, portability, and suitability for point-of-care testing platforms. PABA was selected as the functional polymer due to its conducting nature, anti-fouling properties, and pH-adjustable surface chemistry. Although PABA contains both -COOH and -NH_2 functional groups, only the carboxyl group significantly governs the surface charge behavior after electropolymerization. During electropolymerization, the -NH_2 groups are chemically transformed and incorporated into the polymer backbone, losing their free, ionizable nature. Consequently, the pH-dependent electrochemical response of the film is solely attributed to the carboxyl moieties ($\text{pK}_a \approx 4.5$), while the amine-derived structures no longer contribute to surface charge. At the working pH of 8.5, the carboxylic acid groups in PABA are deprotonated to -COO^- , creating a negatively charged electrode surface. This electrostatic environment helps repel other negatively charged molecules, such as ascorbic acid and BR degradation products, reducing fouling and enhancing the selectivity toward BV oxidation. In addition, PABA acts as a spacer layer, minimizing protein adsorption from complex biological samples such as serum and increasing the effective electrochemical surface area.

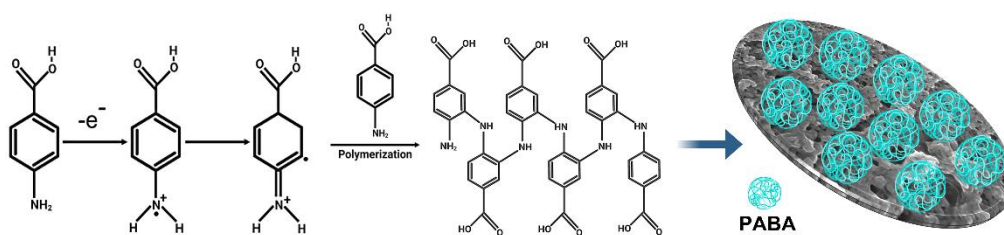


Fig. 5. Electropolymerization mechanism of 4-aminobenzoic acid (4-ABA).

Structurally, the para-substituted amine and carboxyl groups in PABA promote extended π -conjugation in the polymer backbone, which improves charge transfer kinetics and electrocatalytic activity. Compared to other polymers such as polyaniline or poly(3-aminobenzoic acid), PABA provides better film uniformity, pH control, and compatibility with biomolecular sensing.

2.3. Electrochemical Analysis of Biliverdin using SPE/PABA

The electrochemical analysis of BV was carried out using the SPE/PABA-modified electrode. BV is a major biomolecule produced during heme metabolism, and its accurate quantification is important for the diagnosis of various diseases. To achieve this, an electrochemical detection method was selected due to its high sensitivity and rapid response characteristics. The PABA-functionalized electrode was used to promote electron transfer and suppress non-specific adsorption, allowing for selective detection of BV oxidation. CV was first performed to determine the oxidation potential of BV, and based on the results, multiple-pulse amperometric detection (MPAD) was employed to record steady-state current responses across a range of BV concentrations. These data were used to evaluate the linearity, sensitivity, and limit of detection (LOD) of the sensor. In addition, the long-term stability, reproducibility, and selectivity of the sensor were systematically verified, and BV detection in spiked human serum samples was performed to assess practical applicability. Finally, a comparative analysis with a UV-Vis spectrophotometric standard method was conducted to validate the reliability of the developed electrochemical sensing system. Therefore, this part of the study focused on the precise electrochemical analysis of BV using the SPE/PABA electrode and the evaluation of its potential for practical applications.

3. Materials and Experimental

3.1. Chemicals and Reagents

Bilirubin ($\geq 98\%$), gold (III) chloride trihydrate ($\geq 49.0\%$ Au basis), uric acid ($\geq 99\%$), cholesterol, ascorbic acid ($\geq 99\%$), dopamine hydrochloride ($\geq 95\%$), glucose (99.5%), glutathione ($\geq 97\%$), hydrogen peroxide (35%), and 4-aminobenzoic acid (4-ABA) ($\geq 99\%$) were purchased from Sigma-Aldrich, Korea. Tris(hydroxymethyl) aminomethane ($\geq 99\%$) and sodium hydroxide ($\geq 98\%$) were purchased from Samchon Chemical Co., Ltd., Seoul, South Korea. Normal human serum was purchased from (EMD Millipore Corp., USA). $K_4[FeCN_6]$ and $K_3[FeCN_6]$ were purchased from Alfa Aesar, Korea. Analytical grade sodium hydrogen phosphate, sodium dihydrogen phosphate, sodium acetate, and acetic acid were used without further purification. All experiments were conducted using ultrapure Milli-Q-water (≤ 18.2 M Ω .cm) acquired from Human Power I⁺.

3.2. Instrumentation

Electrochemical measurements were carried out using the EmStat4R electrochemical analyzer (PalmSens, Netherlands), which functions as a potentiostat, galvanostat, and impedance analyzer, employing a standard three-electrode setup. Commercial screen-printed carbon electrodes (SPEs, Italsens IS-C) were obtained from PalmSens (Seoul, South Korea). Each SPE was fabricated on a flexible polyester substrate with printed carbon serving as both the working and counter electrodes, while silver ink was used for the reference electrode. The working electrode surface area was approximately 0.076 mm². Modification of the SPE surface was performed using poly(4-aminobenzoic acid).

The functionalization of the electrode was confirmed using a dispersive Micro-Raman spectrometer (JASCO NRS-5100, JASCO International, Japan), operated with a 532.06 nm laser at a power of 4.8 mW. Surface features and composition were

evaluated via field-emission scanning electron microscopy (FESEM, JEOL JSM-6700F) coupled with energy-dispersive X-ray spectroscopy (EDS). UV-Vis absorption data were collected using an Epoch microplate spectrophotometer (BioTek Instruments, USA). X-ray photoelectron spectroscopy (XPS) measurements were conducted on a KRATOS AXIS SUPRA system (Kratos Analytical Ltd., UK) using an Al K α X-ray source (1486.69 eV) at 225 W under angle-resolved conditions. For liquid-phase mass analysis, LC-MS/MS was performed using a Waters ACQUITY UPLC system integrated with a SCIEX triple quadrupole mass spectrometer, operated in positive ion mode with a Turbo IonDrive electrospray interface.

3.3. Au³⁺-Assisted Bilirubin Oxidation

3.3.1. UV-Vis Spectroscopy Analysis

UV-Vis spectroscopy was employed to investigate the oxidation of BR in the presence of Au³⁺. A 3 mL solution of 1 mM BR was initially prepared in ethanol containing 60 μ L of 0.1 M NaOH to ensure complete solubility. A series of reaction mixtures was then prepared (Fig. 6) by maintaining a fixed Au³⁺ concentration at 100 μ M while varying BR concentrations from 10 μ M to 70 μ M. Each mixture was stirred at room temperature for 5 minutes to initiate the oxidation reaction. After incubation, 300 μ L of each reaction mixture was transferred to a 96-well clear flat-bottom plate for spectral measurement. UV-Vis spectra were recorded across the 300–800 nm wavelength range at 2 nm intervals using a multi-mode plate reader equipped with UV-Vis detection capabilities. The concentration prior to the appearance of the BR absorbance peak was further used to identify the molar ratio of the reaction. Additionally, to perform time-dependent analysis of the oxidation process, the absorbance at 700 nm was recorded after initiating the reaction to assess the reaction progress over time. All measurements were conducted under identical optical and environmental conditions to ensure consistency.

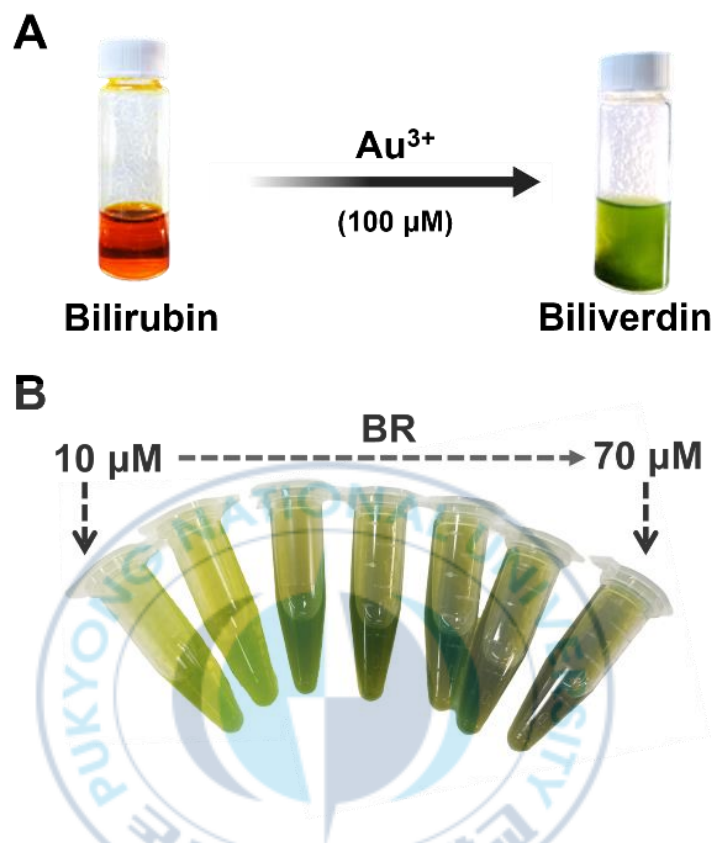


Fig. 6. Photograph of (A) BR oxidation reaction mixture and (B) Reaction mixtures with variable BR concentrations.

3.3.2. LC-MS/MS Analysis

The reaction mixture was analyzed by LC-MS/MS to confirm the formation of biliverdin. The LC-MS/MS analysis was performed using a Waters HSS T3 column ($2.1 \times 50 \text{ mm}$, $1.8 \mu\text{m}$) at 40°C , using mobile phases of 0.1% formic acid in water (A) and 0.1% formic acid in acetonitrile (B) at a flow rate of 0.3 mL/min. The gradient was run over 10 min. The MS was analyzed in MRM mode by monitoring the m/z with a

dwelling time of 150 ms. The gradient elution program was as follows: 0–1 min, 5% B; 1–3.5 min, linear increase to 55% B; 3.5–7 min, increased to 90% B; 7–8 min, 100% B; held at 100% B until 8.01 min; and returned to 5% B by 10 min for re-equilibration. Key MS parameters included the injection volume - 10 μ L, ion spray voltage - 5500 V, temperature - 500°C, and curtain gas - 30 psi.

3.4. Electrochemical Polymerization of 4-ABA into PABA

The electrochemical polymerization of 4-aminobenzoic acid (4-ABA) onto carbon screen-printed electrodes (SPEs) was conducted using a modified procedure based on a previously reported method. This approach aimed at the fabrication of a conductive poly(4-aminobenzoic acid) layer on the electrode surface for electrochemical sensing applications. To evaluate the influence of the number of polymerization cycles on film formation, four individual SPEs were subjected to CV scans of 5, 10, 15, and 20 cycles, respectively. The polymerization was carried out in an aqueous solution of 3 mM 4-ABA in 0.05 M HCl, which served both as the monomer medium and the supporting electrolyte. CV scans were performed over a potential range of 0.1 to 0.8 V at a scan rate of 0.025 V/s in 0.1M HCl. The resulting voltammograms for each cycle number are presented in Fig. 10. Based on these results, 10 cycles were selected as the optimal condition, as justified in Section 4.2.1.

Continuous CV scans were performed using the SPE in 0.05 M HCl containing 3 mM of 4-ABA in the potential range of 0 to 1.2 V at 0.025 V/s for 10 cycles. After the polymerization of poly-aminobenzoic acid on the SPE, the electrode was washed with 0.1 M HCl and water and dried under an N₂ stream. The modified electrode was designated as SPE/PABA and stored in a closed container when not in use.

3.5. Electrochemical Investigation of SPE/PABA

3.5.1. Cyclic Voltammetry (CV)

After polymerization, the electrochemical behavior and surface properties of the SPE/PABA electrode were assessed using CV in varying pH Buffer containing $[\text{Fe}(\text{CN})_6]^{3-/4-}$ to study electron transfer kinetics and surface charge effects under varying protonation conditions. CV measurements were conducted in 0.1 M buffer solutions containing 5 mM of $[\text{Fe}(\text{CN})_6]^{3-/4-}$ with varying pH values ranging from 3.0 to 8.0 to assess the influence of protonation on electron transfer. The CV was recorded within the potential range of 0.1 V to 0.8 V at a scan rate of 0.025 V/s. Redox peak currents and peak-to-peak separations (ΔE_p) were analyzed to evaluate the surface interaction and electrochemical performance of the modified electrode across different pH environments.

3.5.2. Electrochemical Impedance Spectroscopy (EIS)

Electrochemical impedance spectroscopy (EIS) was employed to evaluate the electron transfer characteristics of the poly(4-aminobenzoic acid) (PABA)-modified screen-printed carbon electrode (SPE/PABA). The impedance spectra were recorded in variable pH buffer ranging from 3.0 to 8.0 using appropriate buffer media containing 5 mM of $[\text{Fe}(\text{CN})_6]^{3-/4-}$. EIS measurements were performed at the open-circuit potential (OCP) of each electrode. A sinusoidal voltage perturbation of 5 mV amplitude was applied over a frequency range from 200 kHz to 1 Hz, with 22.8 logarithmically spaced points per decade. Prior to data acquisition, each electrode underwent a stabilization period comprising 10 minutes at OCP.

The impedance spectra were fitted using a modified Randles equivalent circuit consisting of solution resistance, charge transfer resistance, double-layer capacitance, and Warburg impedance, as shown in the inset of the Nyquist plot. Circuit fitting and parameter extraction were carried out using the EmStat4S software. The resulting

impedance spectra were analyzed to extract parameters such as charge transfer resistance (R_{ct}), providing insights into the interfacial electron transfer kinetics and surface properties of the modified electrodes under varying pH conditions.

3.6. Physicochemical Characterization of SPE/PABA

3.6.1. Field Emission Scanning Electron Microscopy (FE-SEM)

FE-SEM analysis was carried out to compare the surface structure of SPE and SPE/PABA. The surface morphology of both bare and modified screen-printed electrodes (SPEs) was investigated using a field emission scanning electron microscope (FESEM)-Schottky type (TESCAN/MIRA3 LMH). The imaging was performed at an accelerating voltage of 10.0 kV using an in-beam secondary electron (SE) detector. High-resolution images were acquired at a magnification of 50.0 kx, providing nanoscale visualization of the modified electrode surface. The resolution at this setting enables detailed assessment of surface morphology and polymer layer distribution. No conductive coating was applied to the samples, as the Schottky emitter allowed for stable imaging under high vacuum conditions.

Elemental analysis was conducted using the EDS (Energy Dispersive X-ray Spectroscopy) system integrated with the FESEM. EDS spectra and elemental mapping were acquired to confirm the presence of nitrogen and other characteristic elements related to the polymer modification. EDS was operated at an accelerating voltage of 10.0 kV, and data acquisition was performed using the instrument's dedicated software for quantitative analysis.

3.6.2. Raman Spectroscopy

Raman spectroscopy was conducted to characterize the chemical structure and surface functionalization of the screen-printed electrodes (SPEs) using a dispersive micro-Raman spectrometer (JASCO NRS-5100). A 532.06 nm laser was used as the excitation source, operating at a power of 4.8 mW. The laser beam was focused on the sample surface using an MPLFLN 100X objective lens. Measurements were performed with an exposure time of 10 seconds and 3 accumulations to enhance the signal-to-noise ratio. The grating used was 600 lines/mm, with a single monochromator setup, a slit size of 25 * 1000 μm , and an aperture of d-4000 μm . A 30/70 beam splitter (BS) and 532.0 nm edge rejection filter were applied to isolate Raman scattering.

Spectra were acquired in the range of 400–4000 cm^{-1} with a spectral resolution of 3.33 cm^{-1} and a data interval of 0.1 cm^{-1} . The system was equipped with a DU420-OE CCD detector cooled to $-59.0\text{ }^{\circ}\text{C}$ to minimize thermal noise, and cosmic ray reduction was enabled. Calibration was performed using a silicon standard. All spectra were collected in backscattering geometry and processed using JASCO's software to identify characteristic vibrational modes of the polymer-modified surface.

3.6.3. X-ray Photoelectron Spectroscopy (XPS)

X-ray photoelectron spectroscopy (XPS) was employed to examine the surface composition and chemical states of both the SPE) and SPE/PABA using a KRATOS AXIS SUPRA spectrometer (Kratos Analytical Ltd., UK) equipped with a monochromatic Al $K\alpha$ X-ray source (1486.6 eV), operating at 225 W with an emission current of 15.00 mA. The system utilized a slot collimator and hybrid lens configuration, with an energy resolution setting of 40. Charge compensation was applied using an electron flood gun (filament current: 0.32 A; bias: 1 V; charge balance: 3.2 V) to minimize surface charging effects.

High-resolution scans were performed over energy windows of 20–22 eV for selected elemental regions using a step size of 0.025 eV, with 800–880 steps per scan and a dwell time of 50 ms per point. Each scan was repeated four times and averaged to enhance spectral quality. All spectra were acquired under ultra-high vacuum conditions at 0° sample tilt. Spectral deconvolution and chemical state analysis were performed using CasaXPS software, with binding energies calibrated against the C 1s peak at 284.8 eV. This analysis enabled qualitative and semi-quantitative evaluation of surface modification and elemental composition changes resulting from PABA functionalization.

3.7. Electrochemical Oxidation of Biliverdin using SPE/PABA

3.7.1. pH Effect on Electrochemical Oxidation of Biliverdin

CV was performed using SPE/PABA to assess the effect of pH on the electrochemical oxidation of BV. Buffer solutions ranging in pH from 3.0 to 8.5 were freshly prepared and analyzed under the same conditions. CV measurements were performed in the potential range of 0.0 to 0.8 V at a scan rate of 0.025 V/s. The anodic peak current and peak potential were extracted from the CV curves, and plots of I_p vs. pH and E_p vs. pH were constructed to identify the optimal pH for BV oxidation.

3.7.2. Cyclic Voltammetry

To evaluate the effect of PABA surface modification on the electrochemical oxidation of BR and BV, the CV response was recorded using both bare SPE and SPE/PABA electrodes. Firstly, the CV response for BR oxidation was recorded using both SPE and SPE/PABA electrodes. Later, the CV response for BV oxidation was similarly recorded using SPE and SPE/PABA. All measurements were conducted using 100 μ M of either BR or BV. The potential was scanned from 0.0 to 0.8 V at a scan rate of 0.025 V/s. For each condition, freshly prepared electrodes were used to ensure

surface consistency and avoid cross-contamination. The CV responses were analyzed to compare the peak current and redox behavior of BR and BV at both unmodified and modified electrode surfaces.

To further evaluate the electrochemical response of BV at the SPE/PABA surface, a concentration-dependent CV study was performed. The measurements were carried out in 0.1 M Tris-HCl buffer (pH 8.5) containing BV at concentrations ranging from 0 to 400 μM . The potential range was maintained from 0.0 to 0.8 V at a scan rate of 0.025 V/s. A single SPE/PABA electrode was utilized to examine the BV oxidation on the electrode surface. The electrode was thoroughly cleaned with DI water before assessing a new concentration. The resulting CV responses were used to examine the relationship between BV concentration and peak current, enabling the evaluation of the sensitivity and redox performance of the modified electrode.

3.7.3. Amperometry

To evaluate the electrochemical sensing performance of BV, amperometric measurements were performed using SPE/PABA. Amperometry was selected because it enables the selective detection of faradaic currents after the initial decay of non-faradaic (capacitive) currents, resulting in a more stable and reliable signal proportional to analyte concentration. Prior to amperometric measurements, the oxidation potential of BV was identified through CV experiments. Based on the CV results, an applied potential of +0.32 V versus Ag/AgCl was selected to ensure selective oxidation of BV with minimal background interference.

The amperometric measurements were performed by dropping BV solutions at concentrations ranging from 4 to 440 μM were freshly prepared in separate Eppendorf tubes using 0.1 M Tris-HCl buffer (pH 8.5). For each measurement, 50 μL of the BV solution was carefully added onto the electrode surface. Multiple-pulse amperometric

detection (MPAD) was employed to study the linear range, sensitivity, and limit of detection (LOD) of the sensor. Initially, a potential of 0 V was applied for 30 seconds to stabilize the electrode surface and minimize background noise. After 30 seconds, the potential was switched to +0.32 V, and the steady-state current response was recorded. After each measurement, the electrode was thoroughly rinsed with deionized (DI) water to eliminate any residual BV and to prevent cross-contamination between tests. The steady-state current values obtained at different BV concentrations were systematically collected for subsequent calibration curve construction and sensor performance evaluation.

3.8. Specificity Study

Specificity studies are important in the development and validation of electrochemical biosensors to ensure their selectivity, especially when analyzing complex biological samples like human serum. These studies assess the sensor's ability to distinguish the target analyte from other electroactive species that may be present in the sample matrix, ensuring that the measured response is specific to the analyte of interest. To assess the selectivity of the PABA-modified SPE electrode for BV detection, specificity study was conducted by investigating the effect of various electroactive biomolecules commonly present in human serum. The analyzed electroactive biomolecules included uric acid (UA, 10 μ M), cholesterol (Chl, 100 μ M), ascorbic acid (AA, 10 μ M), dopamine (DA, 10 μ M), glucose (Gluc, 100 μ M), glutathione (Glut, 10 μ M), and hydrogen peroxide (H_2O_2 , 10 μ M), each prepared in 0.1 M Tris-HCl buffer (pH 8.5). For the specificity study, 100 μ M BV was mixed with each biomolecule separately, and 50 μ L of the mixture was drop-cast onto the SPE/PABA electrode surface. The amperometric I-t response was recorded at an applied potential of +0.32 V versus Ag/AgCl following the established measurement protocol. The steady-state oxidation current for BV in the presence of each electroactive molecule was monitored

to evaluate any potential signal deviation compared to the response of BV alone.

3.9. Stability and Reproducibility

The long-term stability and reproducibility of electrochemical biosensors are critical parameters for ensuring their practical usability, particularly in real-sample and clinical applications. To evaluate these aspects, the stability and reproducibility of the developed SPE/PABA electrode for BV detection were systematically studied. For stability testing, freshly fabricated SPE/PABA electrodes were used to monitor the current response over a period of 10 days. Stability was assessed by performing amperometric measurements in the presence of 100 μM BV at an applied potential of +0.32 V in 0.1 M Tris-HCl buffer (pH 8.5). Each day, 50 μL of BV solution was drop-cast onto the electrode, and after an initial stabilization at 0 V, the steady-state oxidation current was recorded following the potential switch to +0.32 V. Between measurements, the electrodes were stored under ambient laboratory conditions to simulate practical usage environments.

For reproducibility evaluation, three independently fabricated SPE/PABA electrodes were prepared following identical surface modification protocols. The reproducibility study was conducted by recording the amperometric current responses toward 200 μM BV using the same drop-cast and measurement procedure as used in stability testing. The steady-state currents obtained from each electrode were used to calculate the mean, standard deviation (SD), and relative standard deviation (RSD) to quantify signal consistency. Demonstrating minimal variability among different electrodes is essential to verify the repeatability of the fabrication process and the reliability of the sensor performance, as commonly emphasized in published electrochemical biosensor studies.

3.10. Recovery Study

To evaluate the accuracy and practical applicability of the developed sensor, a recovery study was performed using the SPE/PABA-modified electrode. Amperometric measurements were carried out at a fixed applied potential of +0.32 V in 0.1 M Tris-HCl buffer solution (pH 8.5). Five desirable concentrations of BV (70, 110, 170, 280, and 350 μM) were prepared to simulate real-sample conditions. For each concentration, 50 μL of the BV solution was drop-cast onto the working electrode surface, and the steady-state current response was recorded after stabilization. The recovery percentage was calculated by comparing the measured concentrations, determined from the calibration curve, to the known spiked concentrations. This study was conducted to assess the accuracy and reliability of the sensor in detecting BV at varying concentration levels.

3.11. Real Sample Analysis

Real sample analysis is an essential step in evaluating the practical applicability and reliability of electrochemical biosensors for clinical or diagnostic purposes. Due to the complex nature of biological matrices such as human serum, it is important to verify that the developed sensor maintains its performance in the presence of real sample components without significant matrix interference. To assess the practical performance of the SPE/PABA-modified electrode, real sample analysis was conducted using human blood serum. Human serum samples were initially diluted 100-fold with 0.1 M Tris-HCl buffer (pH 8.5) to reduce the effects of endogenous proteins and ions and to match the electrochemical measurement conditions. Known concentrations of BV were then spiked into the diluted serum to prepare final BV concentrations of 60, 80, 100, and 120 μM . For each test, 500 μL of the diluted serum was mixed with 500 μL of Tris-HCl buffer containing the target concentration of BV, resulting in a total sample volume of 1 mL. Baseline amperometric currents were first recorded from the

diluted serum without BV to serve as control measurements. Following this, 50 μL aliquots of the BV-spiked serum samples were drop-cast onto the working surface of the SPE/PABA electrode, and amperometric measurements were performed at an applied potential of +0.32 V versus Ag/AgCl. The steady-state oxidation currents obtained from these measurements were subsequently used to estimate the BV concentration by referencing the standard calibration curve constructed previously.

3.12. Comparison of Electrochemical Method and Standard Method

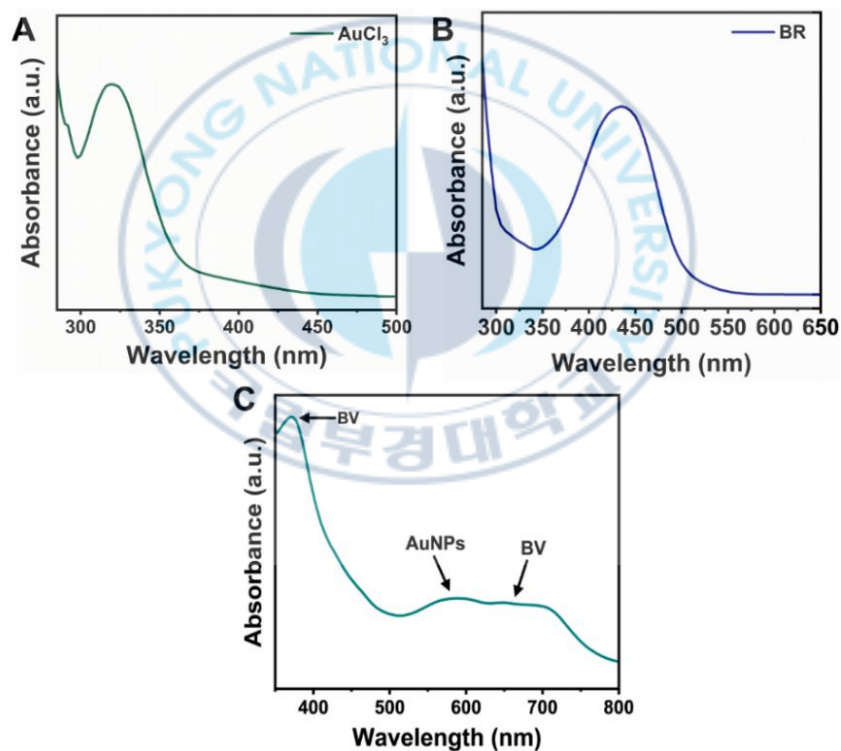
To further assess the reliability and analytical accuracy of the developed SPE/PABA electrochemical sensor for BV detection, a comparative study was conducted using a standard UV-Vis spectrophotometric method. UV-Vis spectroscopy is widely recognized as a conventional and reliable technique for quantitative analysis of biomolecules, providing a suitable benchmark for validating newly developed electrochemical sensors. For the comparison, a standard calibration curve was constructed by recording the UV-Vis absorbance spectra of BV standard solutions prepared at concentrations ranging from 1 to 180 μM in 0.1 M Tris-HCl buffer (pH 8.5). The absorbance measurements were carried out by scanning across the relevant wavelength range, and the absorbance at the maximum characteristic peak of BV was used to develop the calibration plot. The resulting standard curve was then utilized to determine the BV concentrations in spiked human serum samples under the same dilution and preparation conditions used for electrochemical analysis. This comparative analysis allowed for the evaluation of the sensor's accuracy against an established standard method.

4. Results and Discussion

4.1. Analysis of Bilirubin Oxidation Reaction

4.1.1. UV-Vis Spectroscopy Analysis

The UV-vis spectra were separately recorded for $\text{AuCl}_3 \cdot 3\text{H}_2\text{O}$ and BR in ethanol, the results showed maximum absorbance at 290 and 430 nm, respectively (Fig. 7 A & B). Then, the BR oxidation in the presence of Au^{3+} was performed in ethanol medium and a photograph of color changes of the reaction mixture from orange to green was



shown in Fig. 6A and Fig. 6B corresponds to variable BR concentration in the reaction.

Fig. 7. UV-visible spectrum of (A) Ethanolic solution of gold chloride, (B) Ethanolic solution of BR, and (C) After completion of the reaction mixture of Au^{3+} and BR.

The UV-vis spectra of the reaction mixture (Fig. 7C) showed the formation of AuNPs (580 nm) and BV (370 nm, 600 to 700 nm). These λ_{\max} values for Au^{3+} , BR, and the reaction mixture are consistent with the previously reported literature [27–30]. Through trial-and-error experiments, 100 μM of Au^{3+} was selected for the reaction with BR concentrations from 10 μM , and UV-vis spectra were recorded (Fig. 8A). The absorbance spectra of gold (III) chloride trihydrate in the presence of BR reveal that the BR absorbance at 430 nm disappeared, with a broad peak emerging at 370 nm and another broad peak from 600 to 700 nm, corresponding to BV formation [31,32]. Further, these peaks increased with BR concentrations, and the peak at 430 nm reappeared beyond 60 μM of BR which indicates the saturation of the reaction. The complete oxidation of 60 μM BR was confirmed by the absence of the BR characteristic peak at 430 nm.

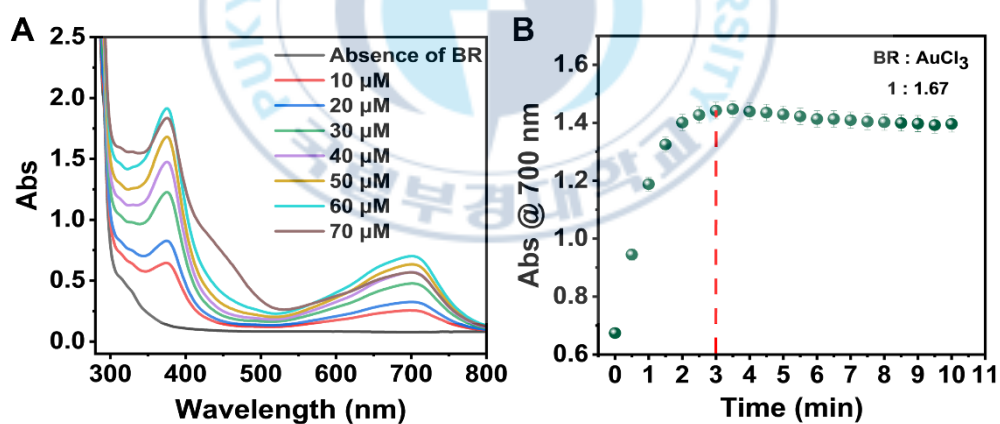


Fig. 8. UV-visible spectrum (A) Absorbance spectra with variable BR concentrations (10 to 70 μM) and (B) Time-dependent absorbance curve at 700 nm. The reactions were performed in the presence of gold (III) chloride (100 μM) in an ethanolic solution.

The formation of BV was further validated through electrochemical analysis, which is explained in section 3.4. Further, the BR: Au³⁺ molar ratio was calculated to be 1:1.67. The time-dependent absorbance at $\lambda_{\text{max}} = 700 \text{ nm}$ was recorded for the reaction between BR and Au³⁺(Fig. 8B). to monitor BV formation. It can be noted that the time required for the complete BR oxidation into BV is $\leq 3 \text{ min}$ at a molar ratio of 1:1.67. Thus, BR oxidation reactions were performed for 5 min throughout this study to ensure completion of the reaction.

4.1.2. LC-MS/MS Analysis

The LC-MS/MS analysis was performed to characterize the reaction mixture. Initially, biliverdin standard (commercial) solution in ethanol was analyzed using LC-MS/MS and the corresponding chromatogram and mass fragmentation are shown in Fig. 9. The Blue and red curves represent the relative abundance of the standard biliverdin solution and the reaction mixture, respectively.

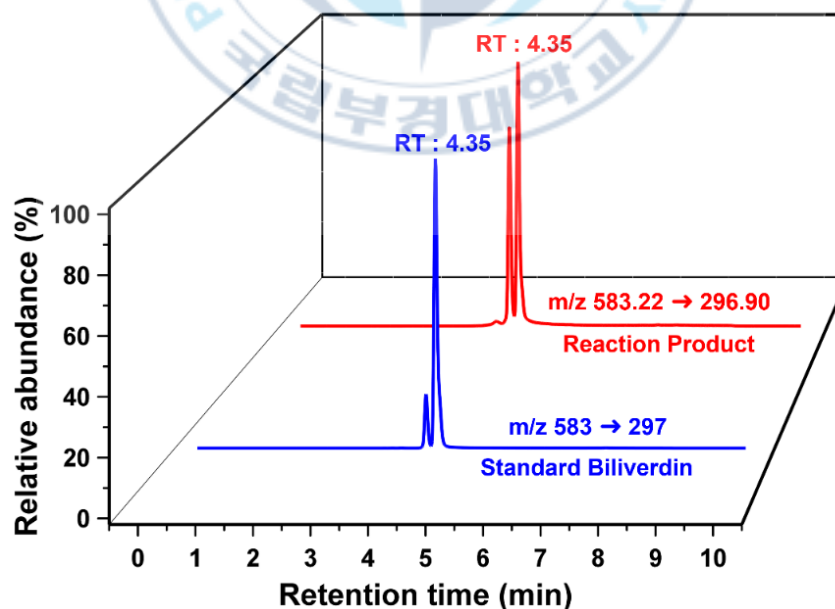


Fig. 9. LC-MS/MS chromatograms of standard biliverdin (blue chromatogram) and the reaction product (red chromatogram). Both compounds eluted at a retention time of 4.35 min, confirming that the product formed in the reaction matches the standard biliverdin.

The ethanol was eluted at RT = 4.17 minutes and followed by BV elution at 4.35 minutes. The molecular ion fragment of the biliverdin standard sample had the mass of 583 and the fragments of m/z 297 was observed. These findings also coexisted with previous reports. Subsequently, the BR oxidation reaction mixture was subjected to LC-MS/MS, and the molecular ion fragmentation to fragments was observed from m/z 583.22 to 296.90 at the same retention time (RT) of 4.35 minutes. The elution time at 4.35 minutes for the BR oxidized product confirms the biliverdin formation.

4.2. Electrochemical Investigation of SPE/PABA

4.2.1. Cyclic Voltammetry (CV)

The sensor electrode was fabricated by the electrochemical polymerization of 4-ABA on carbon SPE by the potential dynamic technique. The CVs were performed using the SPE in 0.05 M HCl containing 3 mM of 4-ABA between 0.0 and 1.2 V at 0.025V/s. Variable cycling scans of 5, 10, 15, and 20 were performed to optimize the 4-ABA polymerization on the SPE, and the modified electrode (SPE/PABA) was evaluated by CV in 0.1 M HCl (Fig. 10).

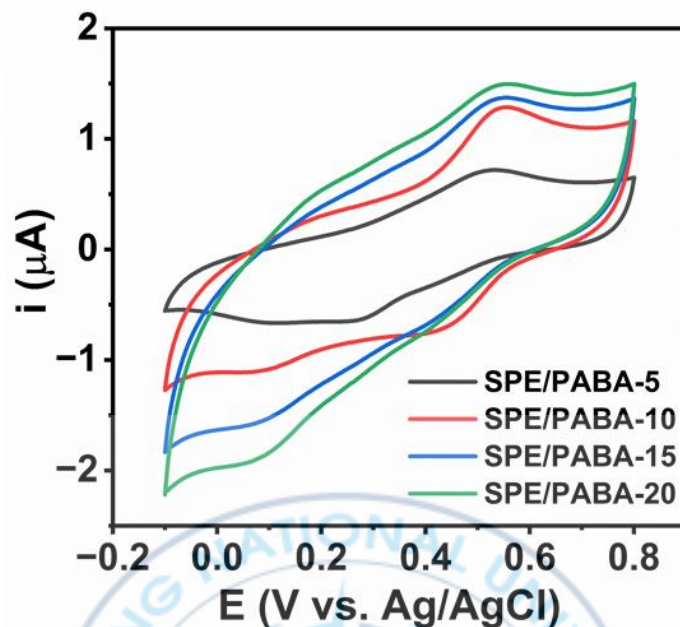


Fig. 10. CV curves were recorded using SPE/PABA modified electrodes in 0.1 M HCl at 25 mV s^{-1} . The Inset label indicates the various cycling scans (5, 10, 15 and 20 scans) during the polymerization of PABA on SPE.

Fig. 10 exhibited two redox peaks at 0.54/0.44 V and 0.17/0.10 V. The first redox peak corresponds to a one-electron transfer, while the second redox peak corresponds to a two-proton and one-electron transfer process. These electrochemical and redox behaviors of amine-containing polymers are well documented and coexist with earlier studies [33,34]. The electrochemical polymerization with 10 cycling scans showed a maximum Faradaic redox peak current with a lower double-layer capacitance compared to the other polymerization cycling scans. Therefore, an SPE/PABA-modified electrode with 10 cycling scans was used for further experimental investigations in this study.

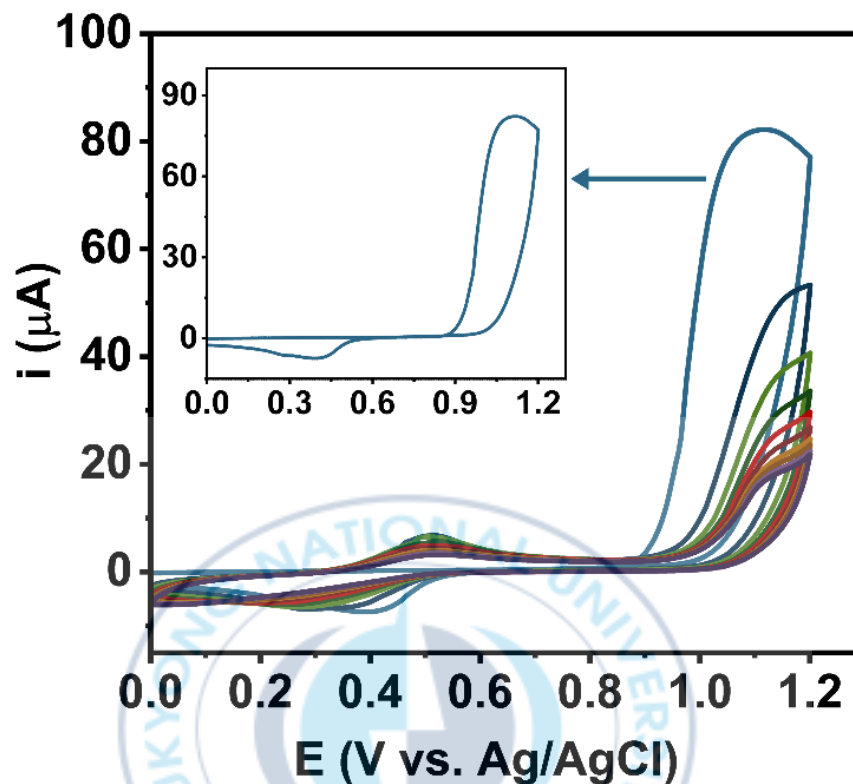


Fig. 11. Electrochemical polymerization on SPE in 0.05 M HCl with 3 mM 4-ABA at 0.025 V/s over ten cycling scans.

The electropolymerization of 4-ABA on SPE is shown in Fig. 11. In Fig. 11, the first scan of polymerization, 4-ABA is oxidized to form radical cation initiation at 1.1 V, and in the cathodic scan, a reduction peak is obtained at 0.4 V [35]. On subsequent scans, a new anodic peak is obtained at $E_{pa} = 0.5$ V, and the peak current gradually increases with cycling scans. Meanwhile, the oxidation peak potential at 1.1 V is insignificantly shifted to a more positive region with a decrease in current. The redox peak current increases with the number of potential scans, confirming the polymerization of 4-ABA into poly-ABA (PABA) and its behavior as a conducting polymer, which agrees with previous reports [36].

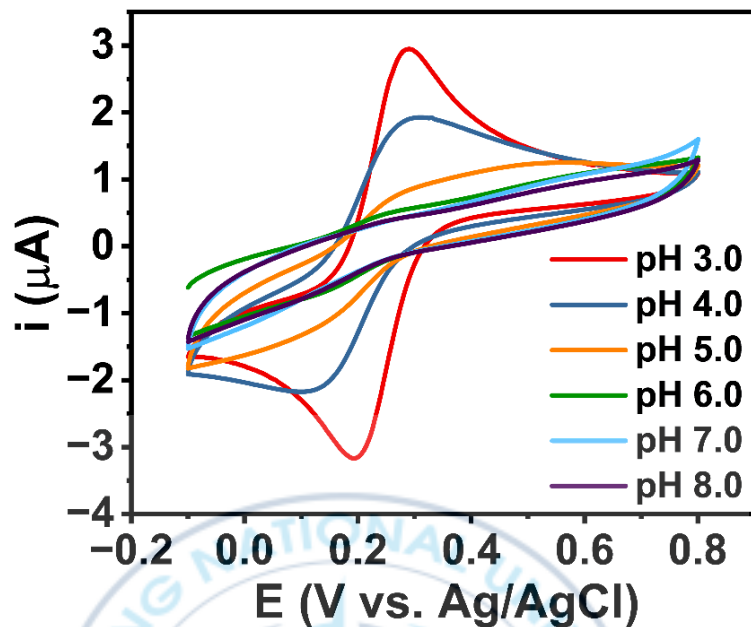


Fig. 12. CV response obtained using SPE/PABA in variable pH buffered solution containing 5 mM of $K_4[FeCN_6]/K_3[FeCN_6]$.

After successful polymerization, the electrochemical behavior and surface nature of the SPE/PABA electrode were investigated in the presence of negatively charged redox species ($[Fe(CN)_6]^{3-/4-}$) in variable pH buffer. The CV (Fig. 12) showed a well-defined redox peak with $\Delta E_p = 95$ mV in pH 3 buffer containing $[Fe(CN)_6]^{3-/4-}$. As pH increases, the redox peak current dramatically dropped with increasing ΔE_p and this electrochemical behavior coexisted with the previous study [37]. The surface $-COOH$ group of the SPE/PABA electrode has a pK_a value of 4.5; below this pH, the $-COOH$ group is protonated to form a positively charged surface that attracts anionic redox molecules. At a pH above 5, $-COOH$ exists as a negatively charged surface which repels the redox molecule and leads to slow electron transfer.

4.2.2. Electrochemical Impedance Spectroscopy (EIS)

EIS analysis was conducted to assess the electrochemical kinetics and surface properties of the SPE/PABA electrode in variable pH buffer containing an anionic redox probe ($[\text{Fe}(\text{CN})_6]^{3-/4-}$). The complex plane impedance plots of the SPE/PABA electrode are shown in Fig. 13A, and the corresponding R_{ct} values with pH are in Fig. 13B. In the case of $\text{pH} = 3$, a semicircle observed in the high-frequency region, followed by a straight line in the low-frequency region indicates a diffusion-controlled process associated with the redox probe (enlarged view of Fig. 13A, inset).

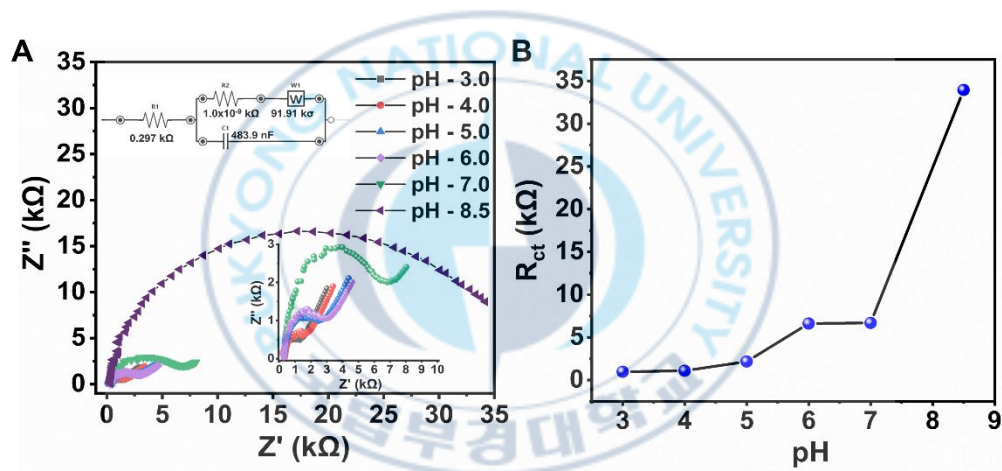


Fig. 13. EIS curves obtained using SPE/PABA in variable pH buffered solution containing 5 mM of $\text{K}_4[\text{FeCN}_6]/\text{K}_3[\text{FeCN}_6]$, Inset of (A) is the equivalent circuit obtained from fitting, and (B) shows the Effect of pH on R_{ct} .

In contrast, the semicircle was increased with increasing pH of the buffer with very little diffusion, suggesting a complete blocking behavior for the electron transfer reaction. This behavior also indicates complete charge-transfer control for the redox couple and is correlated with the CV studies in Fig. 13B. The charge transfer resistance (R_{ct}) was calculated using comparable circuit fitting for kinetic analysis and was illustrated in the inset of Fig. 13A. The R_{ct} value in pH 3 was determined to be 0.98

K Ω and further it increased to 33.94 K Ω in pH 8.5. Charge-based interactions and pK_a values lead to slower kinetics and restricted electron transport. At pH 8.5, fully dissociated carboxyl groups create negative charges, further blocking electron flow.

4.3. Physicochemical Characterization of SPE/PABA

4.3.1. Field Emission Scanning Electron Microscopy (FE-SEM)

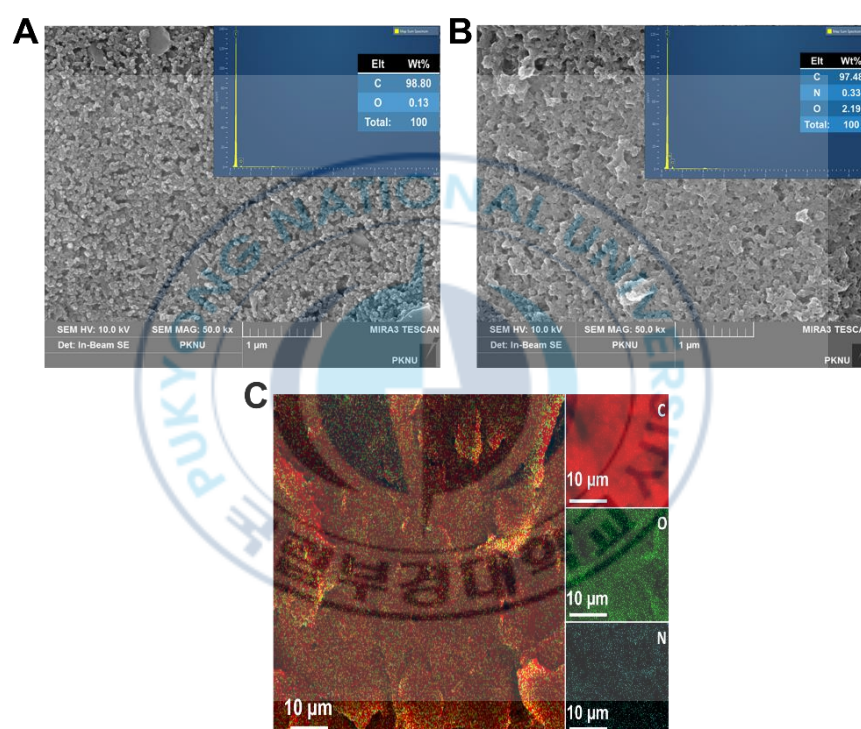


Fig. 14. Physicochemical characterization of the modified electrode. (A) FESEM images of SPE and (B) SPE/PABA electrode; Inset of the fig. (A and B): Elemental analysis. (C) Elemental mapping of the SPE/PABA electrode.

Fig. 14 A&B show the surface morphological nature of the SPE and SPE/PABA obtained from field emission scanning electron microscopy (FE-SEM). Bare SPE has granular carbon particles, and after the polymerization of PABA, the layered polymer

was noted. The elemental analysis from FE-SEM analysis also confirms the PABA by showing the presence of nitrogen (0.33 % wt.), and increasing the weight percent of oxygen to 2.19 % further confirms the polymerization (Inset of Fig. 14A &B). Energy dispersive X-ray (EDX) and elemental mapping analysis for the dispersion of the PABA deposited on the SPE are shown in Fig. 14C. The Inset of Fig. 14C shows the nature of the element mappings for a selected specimen area, revealing a homogeneous distribution of C, O, and N on the SPE. Generally, the brighter the color appears, the higher the concentration of the specific element.

4.3.2. Raman Spectroscopy

Raman spectroscopy is an important approach for the structural characterization of carbon-based nanomaterials [38]. The principal feature in the Raman spectra of modified electrodes consists of two characteristic peaks within the 1300–1600 cm^{-1} [39] range and is referred to as the D and G bands, respectively. Fig. 15 shows the Raman spectra of the SPE and SPE/PABA electrode surfaces. The Raman spectrum of the modified electrode shows two strong peaks corresponding to the disorder (D) and graphitic (G) bands [40]. The D band at 1333 cm^{-1} represents defects and disorder in the sp^2 carbon lattice, whereas the G band near 1572 cm^{-1} represents the graphitic character and highly structured organization of sp^2 carbon [41]. A 2D Band was also observed at 2709 cm^{-1} . The ID/IG ratios of the SPE and SPE/PABA were calculated to be 0.79 and 0.91, respectively. The increase in the intensity ratio of ID/IG indicates the presence of PABA on the SPE surface.

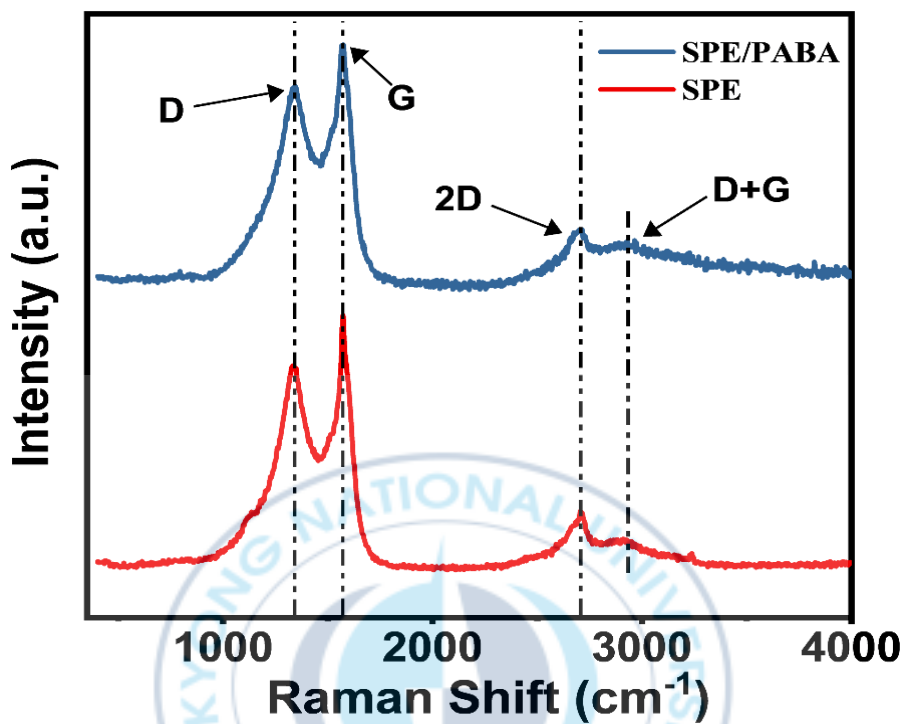


Fig. 15. Raman shift of SPE (red curve) and SPE/PABA (blue curve) surfaces.

4.3.3. X-ray Photoelectron Spectroscopy (XPS)

XPS analysis provided a comprehensive understanding of the elemental composition of the material surface and the binding states of the elements. The XPS spectrum of bare SPE (Fig. 16A) exhibits carbon (94.3%) and oxygen (5.7%). The C1s spectra (Fig. 16B) show the elemental composition of C=C and C–C at 284.5 and 285.3 eV. The peaks at 285.5, 286.6, and 289.0 eV appeared owing to the presence of C–O, C=O, and COOH, respectively [42–44]. The deconvoluted O1s spectrum (Fig. 16C) revealed the peaks for C–O and C=O at 530.7 eV and 531.9 eV, respectively.

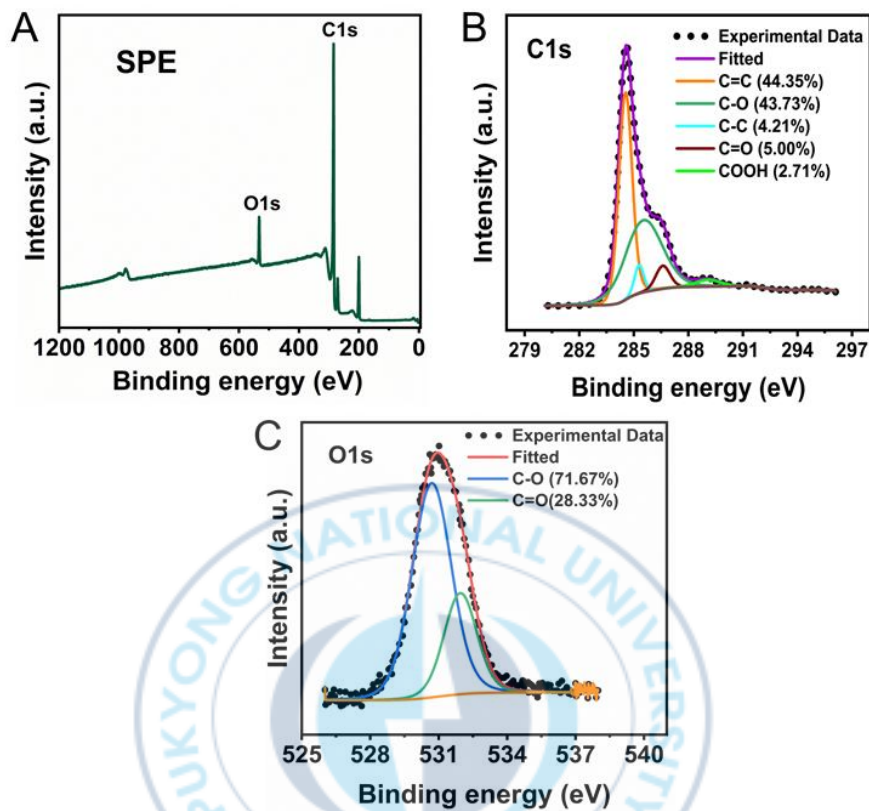


Fig. 16. XPS spectra of SPE electrode (working electrode surface). (A) Survey scan, (B) and (C) High-resolution deconvoluted spectra of C1s and O1s.

The XPS spectra obtained for modified SPE/PABA are shown in Fig. 17A-D. Fig. 17A shows a survey scan of SPE/PABA, indicating the presence of nitrogen, which was obtained from PABA. The deconvoluted C1s, O1s, and N1s spectra are shown in Fig. 17(B-D). In the C1s spectrum, the C=C and C–C peaks were observed at 284.2 and 284.8 eV, respectively.

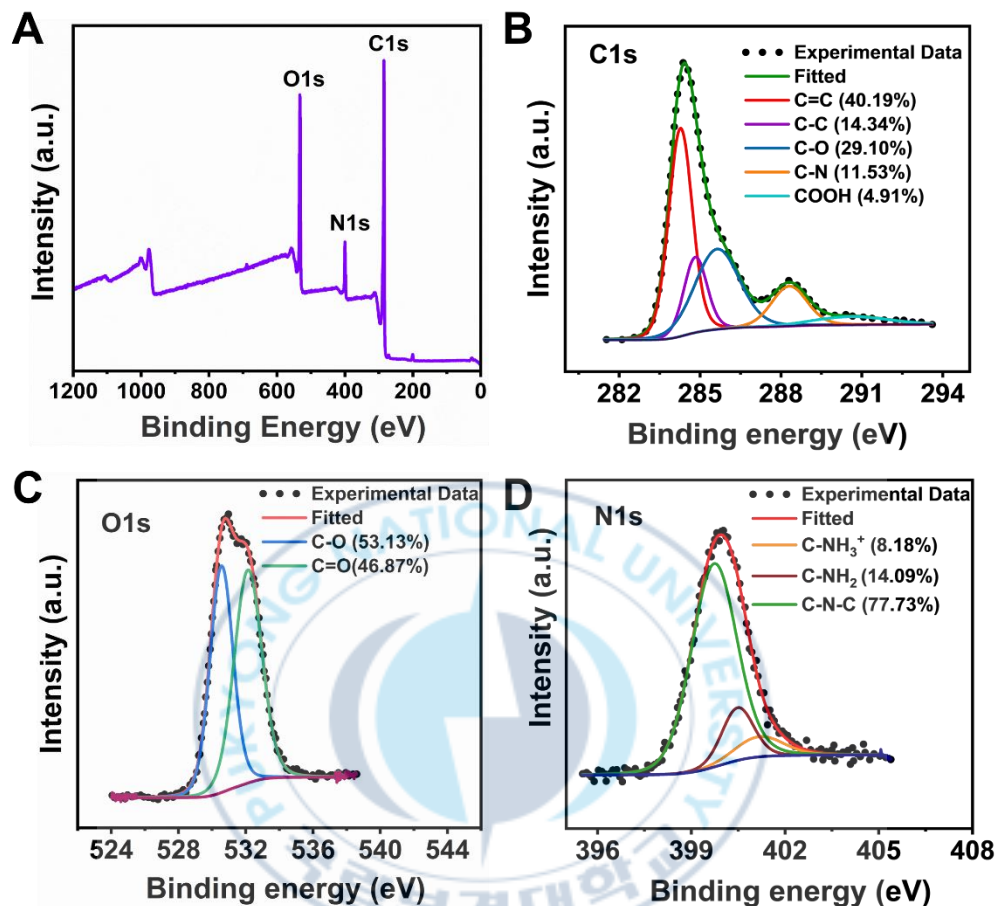


Fig. 17. (A) XPS Survey Scan of SPE/PABA and deconvoluted XPS spectrum of (B) C1s, (C) O1s, and (D) N1s.

The peaks at 285.6, 288.3, and 290.6 eV appear owing to the presence of C–O, C–N, and COOH, respectively [45]. While comparing the C1s spectra of SPE and SPE/PABA, the percentage of COOH was higher (4.91%) than the bare SPE (2.71%), and a new component, the C–N bond, was observed. The increased COOH intensity and the presence of C–N validated the successful electrochemical modification of PABA. The deconvoluted O1s spectrum is shown in Fig. 17G, where C=O and C–O were observed at 532.1 eV and 530.5 eV, respectively [46,47]. In the deconvoluted N1s

(Fig. 17D) spectra, the peaks at 399.7, 400.5, and 401.2 eV are attributed to the C–N–C bond, C–NH₂ group, and the protonated nitrogen species (C–NH₂⁺), respectively [48]. These three components are related to the amino group of PABA. The small areas for the C–NH₂ and C–NH⁺ groups indicate its protonation after adsorption on the SPE. The additional protons may originate from moisture, transfer of a proton within the same molecule (intramolecular), or between different molecules (intermolecular) of the carboxylic acid [49,50].

4.4. Electrochemical Oxidation of Biliverdin at SPE/PABA Electrode

4.4.1. pH Effect on Electrochemical Oxidation of Biliverdin

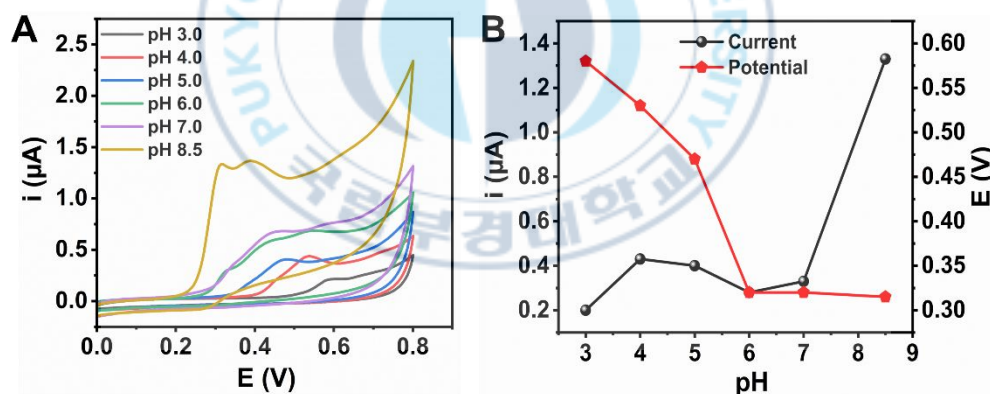


Fig. 18. Electrochemical oxidation of BV at the SPE/PABA electrode. (A) CV responses of SPE/PABA electrode in buffer with variable pH containing 150 μM of BV. (B) Effect of pH on peak potential and peak current.

After the oxidation of BR in the presence of Au³⁺, the electrocatalytic oxidation of the obtained BV at the SPE/PABA electrode was investigated. CV studies were performed using SPE/PABA electrodes to observe the effects of the buffer's pH

(3 – 8.5) on the BV electrocatalytic oxidation, and the experimental results are shown in Fig. 18A & B. The SPE/PABA electrode could oxidize BV at all the desired pH levels investigated. Further, the peak potential and current changes were observed with the pH of the buffer. This behavior might be the contribution of proton transfer in the oxidation reaction process. In Fig. 18A, the CVs showed two distinct and irreversible anodic peaks corresponding to the oxidation of biliverdin (BV) to purpurin (PP) to choletelin (Ch.) The BV oxidizes to PP via 2H^+ and 2e^- transfer processes, and PP further oxidizes to Ch through 2H^+ and 2e^- at 0.39 V. The oxidation of BV and its products proceeds through a sequential 2e^- -transfer, resulting in structural transformations with extended conjugated double bonds. Each of these steps involves the concurrent release of protons to enable the conversion of methylene ($-\text{CH}_2$) bridges into unsaturated or carbonyl-containing structures. This coordinated transfer of protons and electrons stabilizes the oxidized intermediates and reflects a mechanism consistent with proton-coupled electron transfer (PCET) [51,52]. The BV oxidation peak potential was shifted from 0.58 to 0.31 V, and the anodic peak current (I_{pa}) was increased from 0.21 to 1.33 μA with pH (3.0 to 8.5). BV oxidation at pH 8.5 exhibited the maximum peak current at a low oxidation potential. At pH 8.5, Tris-HCl buffer facilitates the complete deprotonation and solvation of biliverdin, thereby enhancing its electrochemical mobility and leading to a higher oxidation peak current at a lower potential [53,54]. Therefore, all the electrochemical studies were performed in a Tris-HCl (pH 8.5) buffer solution.

4.4.2. Cyclic Voltammetry

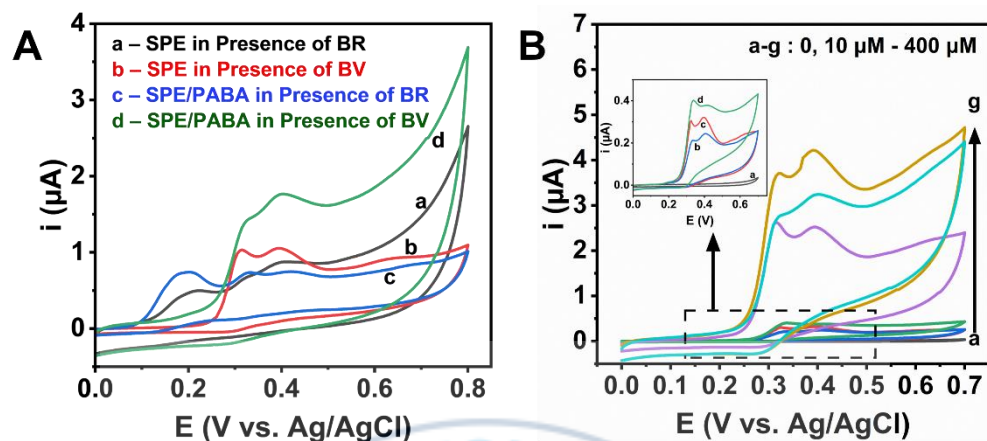


Fig. 19. Electrochemical oxidation of BV at the SPE/PABA electrode. (A) CV responses for a & c in the presence of BR (100 μM), b & d in the presence of BV (100 μM) using SPE and SPE/PABA electrode, and the dotted line correspondence to control CV curve, and (B) CV responses of SPE/PABA modified electrode in Tris-HCL (pH = 8.5) with variable concentrations of BV (0, 10, 20, 50, 200, 300, and 400 μM) at 25 mV s^{-1} (Inset shows enlarged view of CV curves).

Further, CVs were recorded using SPE/PABA electrode in Tris-HCl buffer in the presence of BR and BV (100 μM), and results are shown in Fig. 19A. The bare SPE shows an anodic peak corresponding to BR oxidation at 0.2 V, which correlates with a previous study on carbon surfaces [55] and biliverdin oxidation is observed at 0.32 V. The SPE/PABA modified electrode shows BV oxidation at 0.32 V with a higher current than BR oxidation. However, BR oxidizes at a lower working potential than BV, BR tends to adsorb onto the carbon surface, leading to electrode fouling [25]. This fouling reduces sensitivity and limits the feasibility of direct detection at higher concentrations. This electrode fouling effect leads to a decrease in the sensitivity and limiting direct detection at higher concentrations [56,57]. The bare SPE shows a lower peak current response in the CV for both BR and BV oxidation. By contrast, the SPE/PABA exhibits

a higher oxidation peak current for BV than for BR. Although BR undergoes oxidation on carbon surfaces, it tends to be absorbed onto the electrode surface, leading to the passivation of the electrode. Further, the concentration effects of BV oxidation at SPE/PABA were examined in a 0.1 M Tris buffer in the presence of desirable BV concentrations from 0 to 400 μM at a scan rate of 0.025V/s. Upon the injection of BV, the anodic peak current increased significantly at 0.32 V as shown in Fig. 19B. Furthermore, consistent peak current responses with no broadening or change in working potential provide additional evidence that diffusion and surface kinetics are not adversely affected by BV or its oxidation products. These results confirm that the system retains ideal electrochemical behavior even with increasing analyte concentrations. Thus, the SPE/PABA electrode can be used as a platform for practical applications in determining BV and its correlation with BR for clinical diagnosis.

4.5. Amperometry

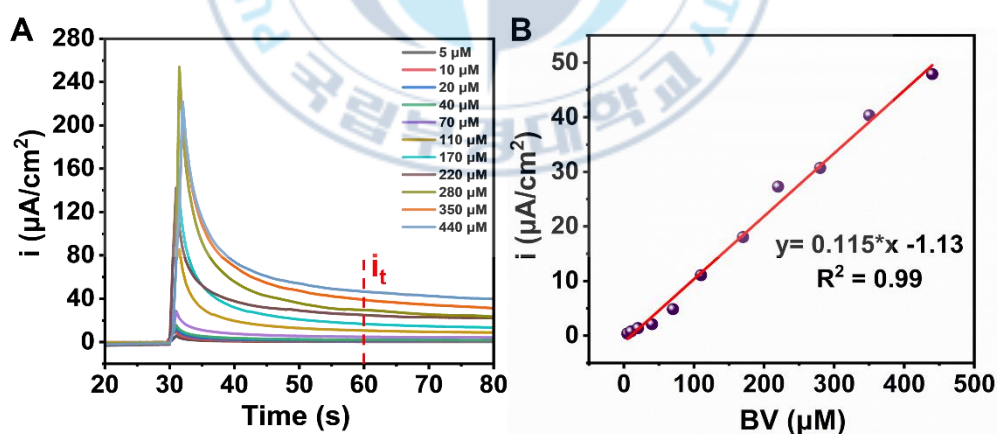


Fig. 20. Electrochemical sensing performance. (A) I–t response recorded using SPE/PABA electrode in the presence of BV concentrations (5 to 440 μM) at 0.32 V and (B) Linearity plot obtained from I–t curves.

To evaluate the sensing performance of BV, the I–t response curve of BV oxidation was recorded using the SPE/PABA electrode at 0.32 V, and the data are shown in Fig. 20A. The BV concentrations were varied from 5 to 440 μM . The I–t curve shows an increase in the steady-state current of BV oxidation and the resultant current density increases with increasing BV concentration, as shown in Fig. 20B. The background current was recorded from the 28th second of the current response to all concentrations before plotting the calibration curve. A calibration plot was obtained with good linearity ($R^2 = 0.9900$) for the BV concentrations studied. The steady-state current (y-axis) obtained at each BV concentration (x-axis) was plotted to generate the calibration curve. The calibration data were fitted using a linear regression model expressed as $y=mx+c$, where y is the measured current, x is the BV concentration, m is the slope, and c is the intercept. The slope (m) of the linear fit represents the sensitivity of the sensor, indicating the change in current per unit concentration, typically expressed in $\mu\text{A}/\mu\text{M}$. A strong linear relationship between current and BV concentration confirmed the reliability of the sensor and demonstrated its quantitative detection capability over the tested concentration range. The linear range was estimated to be 5 to 440 μM with a sensitivity of $0.115 \mu\text{A} \mu\text{M}^{-1} \text{cm}^2$. The limit of detection was calculated to be $0.9 \mu\text{M}$ using $\text{LOD} = 3.3 \cdot \sigma/S$, where σ represents the standard deviation of the sensor's background current response, and S denotes the slope of the linear range of the calibration curve.

The performance and parameters of the developed sensor were compared with those of previously reported BR sensors, as listed in Table 1. Here, the BV sensing performance was compared with that of the BR sensor because the electrochemical sensing of BV has not been reported in the literature. This comparison reveals that the proposed BV sensor outperforms the other sensors in terms of its wider linear range for BV detection, lower working potential, and improved selectivity. According to the literature, although BR oxidizes carbon surfaces, it also causes electrode surface passivation. In this study, we addressed this issue by electropolymerizing 4-ABA. Furthermore, functionalization with 4-ABA enhanced the selectivity and sensitivity of

the sensor and increased mass transport. Therefore, the proposed SPE/PABA surface demonstrated superior sensing performance and characteristic parameters for BV detection compared to other reported materials.

Table 1. Performance comparison with other nonenzymatic electrochemical bilirubin sensors.

Electrode Material	Analyte	Detection Potential (V)	Linear Range (μM)	Detection limit (μM)	Ref.
MIP/Ti ₃ C ₂ T _x MXene/ITO	BR	NR	10–90	0.598	[16]
AuNPs/MWCNT/Fc	BR	0.45	1–100	0.12	[22]
MWCNT–COOH	BR	0.3	0–150	9.4	[58]
Mn–Cu/Nf	BR	0.4	1.2–420	0.025	[59]
GCE/RGO–PSS	BR	0.34	5–315	2	[56]
MIP/HAP/QC	BR	NR	0.05–80	0.01	[60]
CVD Nano graphite/ Platinum microelectrode	BR	0.3	100–500	154	[61]
SPCE	BR	0.25	5–600	NR	[55]
NCs/CBs	BR	0.4	1–100	0.1	[24]
NF/ER-GO	BR	0.7	0–70	0.84	[62]
SPE/PABA	BV	0.32	5–440	0.9	This Work

4.6. Specificity Study

To assess the selectivity of the SPE/PABA electrode for BV detection, other electroactive biomolecules that normally exist in human serum were investigated. The possible electroactive biomolecules presents in human serum (uric acid (UA) - 10 μM , cholesterol (Chl) - 100 μM , ascorbic acid (AA) - 10 μM , dopamine (DA) - 10 μM ,

glucose (Gluc) - 100 μM , glutathione (Glut) - 10 μM , hydrogen peroxide (H_2O_2) - 10 μM) were analyzed in Tris-HCl (pH 8.5) buffer. The I-t response was recorded by amperometry technique and was investigated by monitoring the change in steady state oxidation current for 100 μM BV in the presence of other electrochemically active biomolecules at $E_{\text{app}} = 0.32$ V. The specificity results are shown in Fig. 21A & B. From the results, it can be observed that the steady-state oxidation current for BV was comparatively higher than that for the other biomolecules investigated in this study. AA, DA, and H_2O_2 generated a considerable oxidation current at 0.32 V, but the concentration used in this study was beyond the physiological level in human blood serum. The high specificity was achieved from the anionic surface charge of the SPE/PABA electrode, which repels negatively charged biomolecules, and the optimized applied potential of 0.32 V, at which most common electroactive species do not undergo oxidation. Additionally, PABA modification protects the electrodes against passivation induced by the nonspecific adsorption of proteins and other compounds often found in biological samples, which causes a wide range of BV detection.

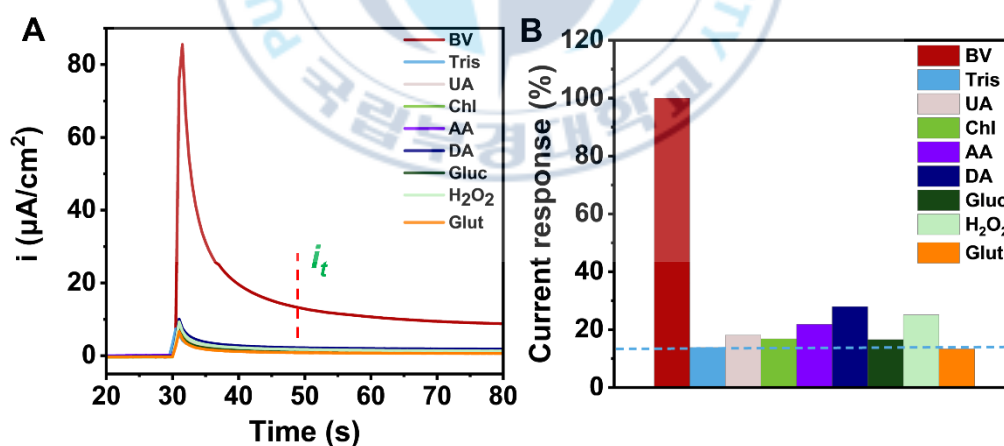


Fig. 21. Electrochemical sensing performance. (A) Selectivity study from I-t response recorded using SPE/PABA electrode with possible electroactive biomolecules, and (B) Histogram representing the relative percentage of current.

4.7. Stability and Reproducibility

The freshly modified SPE/PABA electrodes were used to study the stability and reproducibility performance of the BV sensor. Therefore, the long-term stability of the fabricated sensor electrode was assessed over 10 days. The sensor electrode was subjected to an amperometry study in the presence of BV (100 μM) at 0.32 V in Tris-HCl (Fig. 22A). During this period, the sensor displayed a constant steady-state current for BV oxidation. However, after 10 days, the sensor showed a 1.18% drop in current response, most likely as a result of fouling or surface contamination. Thus, the fabricated SPE/PABA electrode was ideal for BV detection. The electrochemical reproducibility of the sensor electrodes was evaluated by amperometry. Three sensor electrodes were fabricated under the same conditions. The baseline currents were measured to ensure consistency. Subsequently, a known concentration of the BV (200 μM) was introduced, and the current response was recorded over a specified period (Fig. 22B). The mean and standard deviation of the current responses were calculated at each time point, and the relative standard deviation (RSD) was determined to quantify reproducibility.

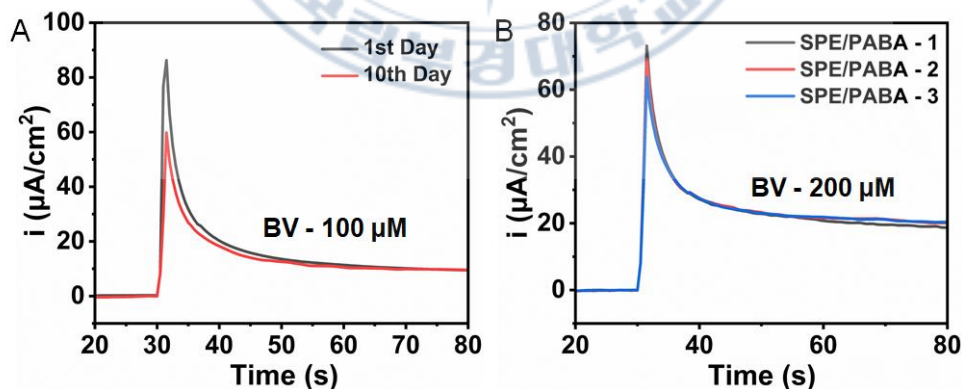


Fig. 22. I-t response curve recorded for (A) Stability (repeatability) and (B) Reproducibility of SPE/PABA modified electrode in Tris-HCl (pH – 8.5) containing BV at 0.32 V.

The results showed an RSD (2.19%) of less than 5%, indicating excellent reproducibility among the three sensor electrodes. Thus, these experimental results revealed that the fabricated SPE/PABA electrode is an excellent sensing platform for BV detection and quantification at near-physiological pH. SPE-based sensing analytical devices are extremely sustainable, affordable, compact, adaptable, and simple to create.

4.8. Recovery Study

The recovery of the SPE/PABA-modified electrode was evaluated using an amperometric technique at an applied working potential ($E_{app} = 0.32$ V) in a Tris-HCl buffer solution. The I-t response curves of five desirable BV samples (70 to 350 μ M) were recorded, and the results are presented in Fig. 23. The current responses for five different BV sample concentrations are listed in Table 2. This study showed a recovery percentage of 98% to 107.8% for the given BV samples, as shown in Table 2, which indicates that the sensor matrix has good recovery values.

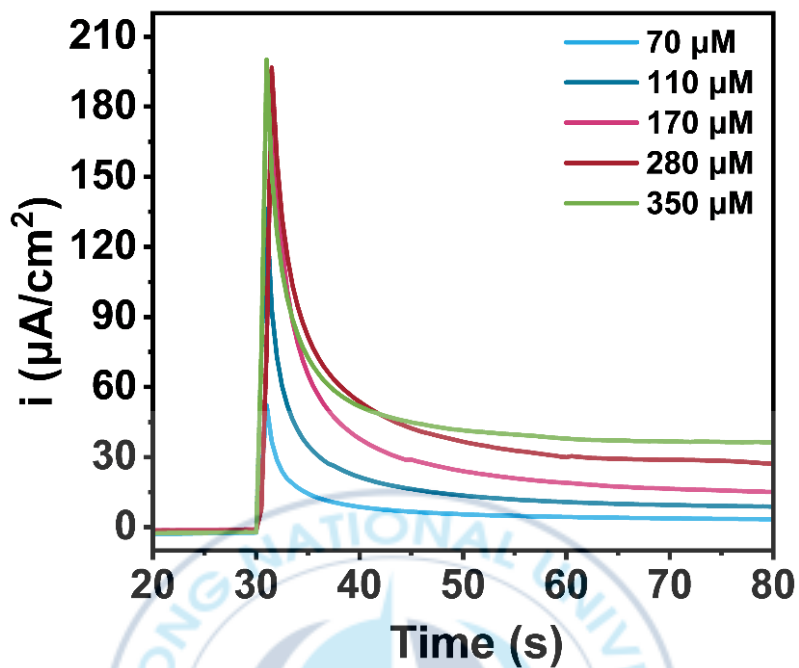


Fig. 23. I-t response curve recorded for variable BV concentration in Tris-HCl (pH 8.5) at 0.32 V.

Table 2. Recovery performance measurement for the added BV using SPE/PABA.

BV Conc. (μM)	Recovered Conc. (μM)	Recovery Performance (%)
70	68.6	98.0
110	115.5	105.0
170	183.3	107.8
280	282.0	100.7
350	358.5	102.4

4.9. Real Sample Analysis

The potential application of the SPE/PABA electrode was evaluated for its practical applicability in blood serum samples. Amperometry was performed on human serum samples spiked with BV. The serum samples were prepared in a Tris-HCl buffer and spiked with four different known concentrations of the BV (60, 80, 100, and 120 μM). Baseline currents were initially measured in serum samples as a control sample. Subsequently, the spiked serum samples were introduced to the buffer, and the current responses were recorded at 0.32 V. The corresponding data are given in Fig. 24, and the analytical results are shown in Table 3. It can be observed from Table 3 that the fabricated sensor matrix exhibited a good recovery percentage for the spiked BV samples. The accuracy and precision of the sensor in detecting analytes in human serum were confirmed by consistent current responses.

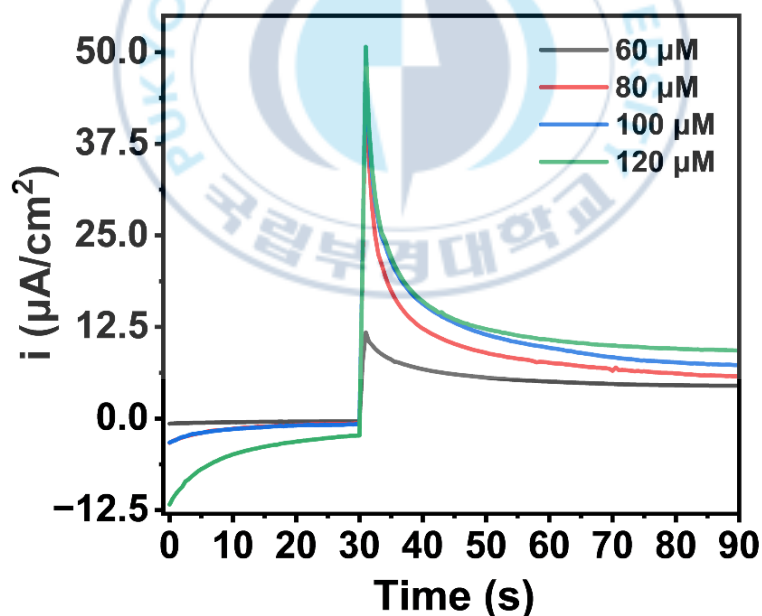


Fig. 24. Electrochemical sensing performance of SPE/PABA in BV-spiked human serum.

Thus, the demonstrated method and electrochemical BV sensor can be reliably used for BV measurements and their correlation with BR concentration in clinical diagnostics. These results indicated that the sensor performed reliably and effectively in complex biological matrices, making it suitable for practical applications in clinical diagnostics.

4.10. Comparison of Electrochemical Method and Standard Method

Further, to evaluate the reliability of the proposed BV sensor, the UV-vis method has been used for the comparison [63,64]. For this, a standardization curve was developed using a BV standard sample at desirable BV concentrations. Fig. 25A-B illustrates the UV-vis spectra and calibration plot obtained using biliverdin (1–180 μM), and the standard curve was used for the detection of the BV sample spiked with human serum. A distinct absorbance peak was observed at $\lambda_{\text{max}} = 670 \text{ nm}$, corresponds to the biliverdin standard, and the absorbance intensity increases proportionally with concentration, indicating a linear concentration-dependent response. Fig. 25B shows the calibration curve obtained at $\lambda_{\text{max}} = 670 \text{ nm}$ with a linear equation of $y = 0.0112 * x + 0.0088$ ($R^2 = 0.9985$). Fig. 25C, the UV-vis spectra of human serum spiked with desirable BV (obtained from the BR oxidation reaction) concentrations (60, 80, 100, and 120 μM) in Tris-HCl buffer and the recovery percentage was calculated using $y = 0.0112 * x + 0.0088$.

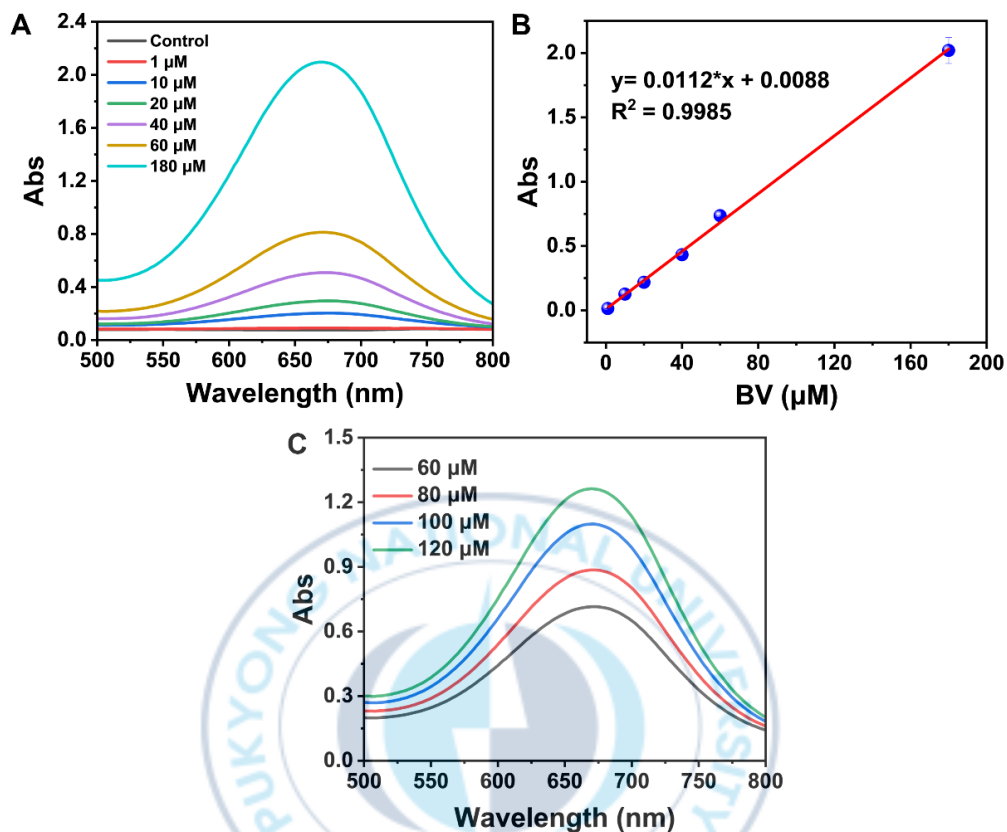


Fig. 25. UV-visible absorbance spectra for (A) Different concentrations (1 to 180 μM) of standard biliverdin, (B) Linearity plot obtained from UV-spectrum, and (C) UV-vis spectral curve recorded for human serum spiked with BV (reaction mixture).

Table 3 shows a comparison of the BV sensing performance of the proposed electrochemical sensing protocol using SPE/PABA electrode and UV-vis based standard method in spiked human serum samples. The experimental results reveal that the proposed electrochemical BV sensor in this work shows satisfactory results, exhibited overall reliability of the BV sensor for diagnosis applications.

Table 3. Comparison of BV sensing performance in spiked human serum samples using SPE/PABA and UV-vis. method.

Spiked BV conc. in human serum (μM)	Proposed electrochemical method (SPE/PABA)		UV-Vis spectroscopy method	
	Recovered conc. (μM)	Recovery performance (%)	Recovered conc. (μM)	Recovery performance (%)
	60	57.04	95.07	56.26
80	81.75	102.19	71.53	89.41
100	100.52	100.52	82.51	82.51
120	123.78	103.15	105.196	87.66

5. Conclusions

This study demonstrates a novel electrochemical sensing approach for BR detection by correlating BV with BR levels. The oxidation of BR to BV by Au^{3+} , followed by its electrochemical oxidation in Tris-HCl buffer (pH 8.5), provides a direct and efficient protocol for electrochemical analysis of BR. This approach addresses the challenges of BR detection, including poor solubility and electrode fouling, ensuring good reproducibility and high selectivity. A poly-aminobenzoic acid-modified screen-printed carbon electrode (SPE/PABA) was used for BV detection, which showed a wide linear range detection, good sensitivity, and high selectivity even in the presence of potential electroactive biomolecules present in human serum. The wide detection range is particularly significant for hyperbilirubinemia diagnosis without electrode passivation, ensuring electrode stability. Moreover, the negatively charged carboxylate on the electrode surface (SPE/PABA) prevents the negatively charged electroactive molecules. Real sample analysis in human serum and recovery studies confirmed the satisfactory findings. Thus, the developed electrode and sensing protocol present a

promising approach for detecting hyperbilirubinemia in clinical diagnosis. Further research is needed to develop total bilirubin sensing methods for point-of-care hyperbilirubinemia testing devices, including the optimization of pH conditions and sample dilution protocols to enable direct analysis of human blood samples. The current proposed platform could serve as a potential route for the clinical diagnosis of BR-related disorders.



6. Reference

- [1] Sticova E, Jirsa M. New insights in bilirubin metabolism and their clinical implications. *World J Gastroenterol* 2013;19:6398–407. <https://doi.org/10.3748/wjg.v19.i38.6398>.
- [2] Narwal V, Batra B, Kalra V, Jalandra R, Ahlawat J, Hooda R, et al. Bilirubin detection by different methods with special emphasis on biosensing: A review. *Sens Biosensing Res* 2021;33:100436. <https://doi.org/10.1016/j.sbsr.2021.100436>.
- [3] Hall B, Levy S, Dufault-Thompson K, Arp G, Zhong A, Ndjite GM, et al. BilR is a gut microbial enzyme that reduces bilirubin to urobilinogen. *Nat Microbiol* 2024;9:173–84. <https://doi.org/10.1038/s41564-023-01549-x>.
- [4] Bulmer AC, Verkade HJ, Wagner KH. Bilirubin and beyond: A review of lipid status in Gilbert's syndrome and its relevance to cardiovascular disease protection. *Prog Lipid Res* 2013;52:193–205. <https://doi.org/10.1016/j.plipres.2012.11.001>.
- [5] Sung KC, Shin J, Lim YH, Wild SH, Byrne CD. Relation of conjugated bilirubin concentrations to the presence of coronary artery calcium. *American Journal of Cardiology* 2013;112:1873–9. <https://doi.org/10.1016/j.amjcard.2013.08.018>.
- [6] Hansen TWR, Wong RJ, Stevenson DK. Molecular physiology and pathophysiology of bilirubin handling by the blood, liver, intestine, and brain in the newborn. *Physiol Rev* 2020;100:1291–346. <https://doi.org/10.1152/physrev.00004.2019>.
- [7] Kazmierczak SC, Robertson AF, Catrou PG, Briley KP, Kreamer BL, Gourley GR. Direct Spectrophotometric Method for Measurement of Bilirubin in Newborns: Comparison with HPLC and an Automated Diazo Method. *Clin Chem* 2002;48:1096–7. <https://doi.org/10.1093/clinchem/48.7.1096>.
- [8] Ndbakuranye JP, Li S, Burchall G, Fox K, Piva T, Xu Z, et al. 70 years of bilirubin sensing: Towards the point-of-care bilirubin monitoring in cirrhosis and hyperbilirubinemia. *Sensors and Diagnostics* 2022;1:932–54. <https://doi.org/10.1039/d2sd00033d>.
- [9] Liu G, Gong Z, Dou X, Li C, Tan Q, Liu Y, et al. An Integrated Electrochemical Sensor with Flexible Microfluidic Structures for Human Sweat Analysis. *Biochip J* 2024. <https://doi.org/10.1007/s13206-024-00181-z>.
- [10] Omar FS, Duraisamy N, Ramesh K, Ramesh S. Conducting polymer and its composite materials based electrochemical sensor for Nicotinamide Adenine Dinucleotide (NADH). *Biosens Bioelectron* 2016;79:763–75. <https://doi.org/10.1016/j.bios.2016.01.013>.
- [11] Ciobanu M, Wilburn JP, Krim ML, Cliffl DE. *Fundamentals*. 2007;3-29. <https://doi.org/10.1016/B978-044451958-0.50002-1>
- [12] Ji W, Tang X, Du W, Lu Y, Wang N, Wu Q, et al. Optical/electrochemical methods for

- detecting mitochondrial energy metabolism. *Chem Soc Rev*, vol. 51, Royal Society of Chemistry; 2022, p. 71–127. <https://doi.org/10.1039/d0cs01610a>.
- [13] Labib M, Sargent EH, Kelley SO. Electrochemical Methods for the Analysis of Clinically Relevant Biomolecules. *Chem Rev* 2016;116:9001–90. <https://doi.org/10.1021/acs.chemrev.6b00220>.
- [14] Elgrishi N, Rountree KJ, McCarthy BD, Rountree ES, Eisenhart TT, Dempsey JL. A Practical Beginner's Guide to Cyclic Voltammetry. *J Chem Educ* 2018;95:197–206. <https://doi.org/10.1021/acs.jchemed.7b00361>.
- [15] Ross PN., Alkire RC., Kolb DM., Lipkowsi Jacek. *Bioelectrochemistry: Fundamentals, Applications and Recent Developments*. John Wiley & Sons, Incorporated; 2013.
- [16] Manoj, Ghreera AS. Ti3C2TxMXene modified indium tin oxide (ITO) electrode for electrochemical sensing of bilirubin based on a molecularly imprinted pyrrole polymer. *Phys Scr* 2024;99. <https://doi.org/10.1088/1402-4896/ad36f6>.
- [17] Manoj, Ghreera AS. Studying the Synergistic Effects of Molecularly Imprinted Orthophenylenediamine and MXene/COOH-MWCNT Composite for Vitro Diagnosis of Bilirubin in Human Serum. *J Appl Polym Sci* 2025. <https://doi.org/10.1002/app.56703>.
- [18] Bui DH, Vu TT, Piro B, Nguyen TTN. Printable FET sensors with using GNH/MnO2 as channel material for non-enzymatic detection of bilirubin. *Diam Relat Mater* 2025;154. <https://doi.org/10.1016/j.diamond.2025.112187>.
- [19] Kumar A, Gupta GH, Singh G, More N, M K, Sharma A, et al. Ultrahigh sensitive graphene oxide/conducting polymer composite based biosensor for cholesterol and bilirubin detection. *Biosens Bioelectron X* 2023;13. <https://doi.org/10.1016/j.biosx.2022.100290>.
- [20] Slifstein CH, Ariel M. The electrochemistry of bilirubin in dimethylsulfoxide. *J Electroanal Chem Interfacial Electrochem* 1973;48:447–63. [https://doi.org/10.1016/S0022-0728\(73\)80377-8](https://doi.org/10.1016/S0022-0728(73)80377-8).
- [21] Mano N, Edembe L. Bilirubin oxidases in bioelectrochemistry: Features and recent findings. *Biosens Bioelectron* 2013;50:478–85. <https://doi.org/10.1016/j.bios.2013.07.014>.
- [22] Wang C, Wang G, Fang B. Electrocatalytic oxidation of bilirubin at ferrocenecarboxamide modified MWCNT-gold nanocomposite electrodes. *Microchimica Acta* 2009;164:113–8. <https://doi.org/10.1007/s00604-008-0041-2>.
- [23] Thangamuthu M, Gabriel WE, Santschi C, Martin OJF. Electrochemical sensor for bilirubin detection using screen printed electrodes functionalized with carbon nanotubes and graphene. *Sensors* 2018;18. <https://doi.org/10.3390/s18030800>.

- [24] Lu ZJ, Cheng Y, Zhang Y, Wang X, Xu P, Yu H, et al. Non-enzymatic free bilirubin electrochemical sensor based on ceria nanocube. *Sens Actuators B Chem* 2021;329. <https://doi.org/10.1016/j.snb.2020.129224>.
- [25] Thangavel B, Lingagouder J, Berchmans S, Ganesh V. Electrochemical grafting of 4-aminobenzoic acid onto toray carbon – Interfacial investigation and fabrication of non-enzymatic bilirubin sensor. *Sens Actuators B Chem* 2021;344. <https://doi.org/10.1016/j.snb.2021.130292>.
- [26] Edachana RP, Kumaresan A, Balasubramanian V, Thiagarajan R, Nair BG, Gopalakrishnan SBT. Paper-based device for the colorimetric assay of bilirubin based on in-situ formation of gold nanoparticles. *Microchimica Acta* 2020;187. <https://doi.org/10.1007/s00604-019-4051-z>.
- [27] Kundu S, Panigrahi S, Praharaj S, Basu S, Ghosh SK, Pal A, et al. Anisotropic growth of gold clusters to gold nanocubes under UV irradiation. *Nanotechnology* 2007;18. <https://doi.org/10.1088/0957-4484/18/7/075712>.
- [28] Alshatteri AH, Omer KM. Smartphone-based fluorescence detection of bilirubin using yellow emissive carbon dots. *Analytical Methods* 2022;14:1730–8. <https://doi.org/10.1039/d1ay02053f>.
- [29] López-Muñoz GA, Balderas-López JA, Ortega-Lopez J, Pescador-Rojas JA, Salazar JS. Thermal diffusivity measurement for urchin-like gold nanofluids with different solvents, sizes and concentrations/shapes. *Nanoscale Res Lett* 2012;7:1–7. <https://doi.org/10.1186/1556-276X-7-667>.
- [30] Haiss W, Thanh NTK, Aveyard J, Fernig DG. Determination of size and concentration of gold nanoparticles from UV-Vis spectra. *Anal Chem* 2007;79:4215–21. <https://doi.org/10.1021/ac0702084>.
- [31] Xiao W, Xiong Y, Li Y, Chen Z, Li H. Non-Enzymatically Colorimetric Bilirubin Sensing Based on the Catalytic Structure Disruption of Gold Nanocages. *Sensors* 2023;23. <https://doi.org/10.3390/s23062969>.
- [32] Ghosh S, Mondal S, Yadav K, Aggarwal S, Schaefer WF, Narayana C, et al. Modulation of biliverdin dynamics and spectral properties by Sandercyanin. *RSC Adv* 2022;12:20296–304. <https://doi.org/10.1039/d2ra02880h>.
- [33] Huang W-S, Humphrey BD, Macdiarmid AG. Polyaniline, a Novel Conducting Polymer Morphology and Chemistry of its Oxidation and Reduction in Aqueous Electrolytes. *J Chem Soc, Faraday Trans 1* 1986;82:2385–400. <https://doi.org/10.1039/F19868202385>.
- [34] Focke WW, Wnek GE, Wei Y. Influence of Oxidation State, pH, and Counterion on the Conductivity of Polyaniline. *J Phys Chem* 1987;91:173. <https://doi.org/10.1021/j100306a059>.

- [35] Qi P, Wang J, Wang X, Wang Z, Xu H, Di S, et al. Sensitive and selective detection of the highly toxic pesticide carbofuran in vegetable samples by a molecularly imprinted electrochemical sensor with signal enhancement by AuNPs. *RSC Adv* 2018;8:25334–41. <https://doi.org/10.1039/c8ra05022h>.
- [36] Ziyatdinova G, Titova M, Davletshin R. Electropolymerized 4-Aminobenzoic Acid Based Voltammetric Sensor for the Simultaneous Determination of Food Azo Dyes. *Polymers (Basel)* 2022;14. <https://doi.org/10.3390/polym14245429>.
- [37] Tekin-Celebi S, Solak AO, Ustundag Z, Demirci S. Determination of pK_a of benzoic acid- and p-aminobenzoic acid-modified platinum surfaces by electrochemical and contact angle measurements. *Chemical Papers* 2012;66:1146–56. <https://doi.org/10.2478/s11696-012-0237-0>.
- [38] Agusti' A, Crevillen AG, Escarpa A, Garci'a CD, Garci'a G. Carbon-based Nanomaterials in Analytical Chemistry. *Detection Science*. 12th ed., The Royal Society of Chemistry; 2018, p. 1–36. <https://doi.org/10.1039/9781788012751-00001>.
- [39] Enache TA, Enculescu M, Bunea MC, Zubillaga EA, Tellechea E, Aresti M, et al. Carbon Inks-Based Screen-Printed Electrodes for Qualitative Analysis of Amino Acids. *Int J Mol Sci* 2023;24. <https://doi.org/10.3390/ijms24021129>.
- [40] Ramaswamy N, Zulevi B, McCool G, Patton N, Shi Z, Chavez A, et al. Engineered Catalyst Support with Improved Durability at Higher Weight Percentage of Platinum. *J Electrochem Soc* 2023;170:114503. <https://doi.org/10.1149/1945-7111/ad0668>.
- [41] Tabrizi AG, Arsalani N, Mohammadi A, Ghadimi LS, Ahadzadeh I. High-performance asymmetric supercapacitor based on hierarchical nanocomposites of polyaniline nanoarrays on graphene oxide and its derived N-doped carbon nanoarrays grown on graphene sheets. *J Colloid Interface Sci* 2018;531:369–81. <https://doi.org/10.1016/j.jcis.2018.07.065>.
- [42] Chiang CL, Yang JM. Flame retardance and thermal stability of polymer/graphene nanosheet oxide composites. *Novel Fire Retardant Polymers and Composite Materials*, Elsevier; 2017, p. 295–312. <https://doi.org/10.1016/b978-0-08-100136-3.00011-x>.
- [43] Chen X, Wang X, Fang D. A review on C1s XPS-spectra for some kinds of carbon materials. *Fullerenes Nanotubes and Carbon Nanostructures* 2020;28:1048–58. <https://doi.org/10.1080/1536383X.2020.1794851>.
- [44] Stando G, Han S, Kumanek B, Lukowiec D, Janas D. Tuning wettability and electrical conductivity of single-walled carbon nanotubes by the modified Hummers method. *Sci Rep* 2022;12. <https://doi.org/10.1038/s41598-022-08343-5>.
- [45] Cherian AR, Benny L, Varghese A, John NS, Hegde G. Molecularly Imprinted Scaffold Based on poly (3-aminobenzoic acid) for Electrochemical Sensing of Vitamin B₆. *J Electrochem Soc* 2021;168:77512. <https://doi.org/10.1149/1945-7111/ac1494>.

- [46] Huang J, Wang W, Wu T, Ren X, Zhao X. Photo-electrochemical activation of persulfate for the simultaneous degradation of microplastics and personal care products. *RSC Adv* 2024;14:16150–69. <https://doi.org/10.1039/d4ra01449a>.
- [47] Havare AK. Thickness Analyses of 4-(Acetyl Amino)-2-Aminobenzoic Acid on ITO Thin Film Using Analytic Based of X-Ray Photoelectron Spectroscopy Method. *Polycycl Aromat Compd* 2023;43:1019–29. <https://doi.org/10.1080/10406638.2021.2023199>.
- [48] Cao L, Huang J, Wu X, Xu Q, Su K, Zhong Y, et al. Boosting and stabilizing the electrocatalytic reduction of carbon dioxide on Bi₂O₂CO₃ via surface modification with p-aminobenzoic acid. *Applied Catalysis B: Environment and Energy* 2024:124451. <https://doi.org/10.1016/j.apcatb.2024.124451>.
- [49] Ohshimo K, Sato R, Takasaki Y, Tsunoda K, Ito R, Kanno M, et al. Highly Efficient Intramolecular Proton Transfer in p-Aminobenzoic Acid by a Single Ammonia Molecule as a Vehicle. *Journal of Physical Chemistry Letters* 2023;14:8281–8. <https://doi.org/10.1021/acs.jpcllett.3c01996>.
- [50] Akasaka K, Hirata K, Haddad F, Dopfer O, Ishiuchi SI, Fujii M. Hydration-induced protomer switching in p-aminobenzoic acid studied by cold double ion trap infrared spectroscopy. *Physical Chemistry Chemical Physics* 2022;25:4481–8. <https://doi.org/10.1039/d2cp04497h>.
- [51] Niu J, Dong S. Investigation on Mechanisms for the Electrooxidation of Some Bile Pigments by Spectroelectrochemistry. *Electroanalysis* 1994;6:437–43. <https://doi.org/10.1002/elan.1140060513>.
- [52] Pradko JR, Pons S, Bandyopadhyay S, Mcaleer JF, Hinman AS. 724—A spectroelectrochemical investigation of the oxidation of bilirubin IX- α in dimethylformamide. *J Electroanal Chem, and Constituting* 1984;13:267–85. [https://doi.org/10.1016/0302-4598\(84\)87031-2](https://doi.org/10.1016/0302-4598(84)87031-2).
- [53] Lightner DA, Holmes DL, McDonagh AF. On the acid dissociation constants of bilirubin and biliverdin: pK_a values from ¹³C NMR spectroscopy. *Journal of Biological Chemistry* 1996;271:2397–405. <https://doi.org/10.1074/jbc.271.5.2397>.
- [54] Tournié A, Majérus O, Lefèvre G, Rager MN, Walmé S, Caurant D, et al. Impact of boron complexation by Tris buffer on the initial dissolution rate of borosilicate glasses. *J Colloid Interface Sci* 2013;400:161–7. <https://doi.org/10.1016/j.jcis.2013.03.009>.
- [55] Raveendran J, Stanley J, Babu TGS. Voltammetric determination of bilirubin on disposable screen printed carbon electrode. *Journal of Electroanalytical Chemistry* 2018;818:124–30. <https://doi.org/10.1016/j.jelechem.2018.04.020>.
- [56] Balamurugan T, Berchmans S. Non-enzymatic detection of bilirubin based on a graphene-polystyrene sulfonate composite. *RSC Adv* 2015;5:50470–7. <https://doi.org/10.1039/c5ra06681f>.

- [57] Wang J, Ozsoz M. A Polishable Amperometric Biosensor for Bilirubin. *Electroanalysis* 1990;2:647–50. <https://doi.org/10.1002/elan.1140020813>.
- [58] Taurino I, Hoof V Van, Micheli G De, Carrara S. Superior sensing performance of multi-walled carbon nanotube-based electrodes to detect unconjugated bilirubin. *Thin Solid Films* 2013;548:546–50. <https://doi.org/10.1016/j.tsf.2013.09.015>.
- [59] Noh HB, Won MS, Shim YB. Selective nonenzymatic bilirubin detection in blood samples using a Nafion/Mn-Cu sensor. *Biosens Bioelectron* 2014;61:554–61. <https://doi.org/10.1016/j.bios.2014.06.002>.
- [60] Yang Z, Zhang C. Molecularly imprinted hydroxyapatite thin film for bilirubin recognition. *Biosens Bioelectron* 2011;29:167–71. <https://doi.org/10.1016/j.bios.2011.08.012>.
- [61] Taurino I, Hoof V Van, Magrez A, Forró L, Micheli G De, Carrara S. Efficient voltammetric discrimination of free bilirubin from uric acid and ascorbic acid by a CVD nanographite-based microelectrode. *Talanta* 2014;130:423–6. <https://doi.org/10.1016/j.talanta.2014.07.009>.
- [62] Avan AA, Aydar S, Filik H. Voltammetric Sensing of Bilirubin Based on Nafion/Electrochemically Reduced Graphene Oxide Composite Modified Glassy Carbon Electrode. *Curr Anal Chem* 2015;11:96–103. <https://doi.org/10.2174/157341101102150223123009>.
- [63] Saleem Q, Shahid S, Rahim A, Javed M, Mansoor S, Zidan A, et al. Enzyme-free electrochemical sensor for dopamine and resorcinol detection using ferrite-polyaniline nanocomposite-decorated glassy carbon electrode. *International Journal of Polymeric Materials and Polymeric Biomaterials* 2025:1–13. <https://doi.org/10.1080/00914037.2025.2453921>.
- [64] Marco A, Canals A, Morallón E, Aguirre MÁ. Electrochemical Sensor for the Determination of Methylthiouracil in Meat Samples. *Sensors* 2022;22. <https://doi.org/10.3390/s22228842>.

Acknowledgement

First and foremost, I would like to express my deepest gratitude to my supervisor, Professor Joong Ho Shin, for his invaluable guidance, patience, and constant support throughout my master's degree. His mentorship helped me to grow not only as a researcher but also as a person. I am truly grateful for the opportunity to learn under his supervision and for the trust he placed in me throughout this journey.

I am also sincerely thankful to Professor Yong Wook Lee and Professor Songyi Lee for giving their valuable time to review my thesis, despite their busy schedules.

I would like to extend my heartfelt appreciation to all members of the Advanced BioMicrosystems Lab (ABML). I am especially thankful to Dr. Balamurugan Thangavel, who has mentored me since the beginning of my master's degree and helped me to understand electrochemistry. My sincere thanks also go to Dr. Bui for his guidance and support during the earlier days at ABML. I am grateful to Han Won, whose consistent encouragement and thoughtful advice helped me move forward through both academic and personal challenges. I am also thankful to SeBeen, JuHee, Minseon, Hyoeun, and Rica for their helpful mind, and for creating a positive lab environment.

Lastly, I would like to express my deepest gratitude to my family for their unconditional love, sacrifices, and unwavering belief in me. Their support gave me the strength and motivation to pursue my goals far from home.

Publications

International Journal

Khan, M. M. R.*, Thangavel, B.*, & Shin, J. H. (2025). Au³⁺-Assisted Bilirubin Oxidation and Electrochemical Investigation of Biliverdin on Poly (4-aminobenzoic acid)-Modified Screen-Printed Carbon Electrode. Journal of The Electrochemical Society.

(*: equally contributed 1st author)

Domestic Conference

Khan, M. M. R.*, Thangavel, B., & Shin, J. H. (2024). Electrochemical Detection of Hyperbilirubinemia via Indirect Sensing of Biliverdin: A Non-Enzymatic Approach. Korea Biochip Society Spring Conference, HICO, Gyeongju, South Korea.

(*Oral Presentation)

Khan, M. M. R.*, Thangavel, B., & Shin, J. H. (2025). Fabrication and Physicochemical Characterization of Poly(4-aminobenzoic acid)-Modified Screen-Printed Electrode for Electrochemical Sensing. Korea Biochip Society Spring Conference, Yeosu, South Korea.

(*Poster Presentation)